Biomass and Bioenergy 196 (2025) 107676

Contents lists available at ScienceDirect

Biomass and Bioenergy

journal homepage: www.elsevier.com/locate/biombioe

An integrated approach to the valorization of pyrolysis products from lignocellulosic residues and by-products

María del Carmen Recio-Ruiz, Ramiro Ruiz-Rosas, Francisco José García-Mateos, María José Valero-Romero, Juana María Rosas, José Rodríguez-Mirasol *, Tomás Cordero

Departamento de Ingeniería Química, Andalucía Tech, University of Malaga, Campus de Teatinos s/n, 29010, Malaga, Spain

ARTICLE INFO

Keywords:
Slow pyrolysis
Lignocellulosic biomass
Syngas
Bio-oil
Biochar
CO_2 adsorption

ABSTRACT

Pyrolysis of biomass waste enables the generation of energy and products, although the sustainability of this process requires an integral valorization of all produced fractions. This paper presents a study on the valorization of all pyrolysis products from selected biomass wastes, such as hemp hurd (HH), olive stone (OS) and almond shell (AS), and two technical lignins, focusing on the effect of the biopolymeric composition on the potential applications of the different pyrolysis streams. The stablished correlation between the lignocellulosic biomass composition and the properties of each of the pyrolysis products obtained (bio-oil, biochar and gases) in relation to their potential applications (in addition to the distribution of pyrolysis products and yields) represents the main novelties of this work. The results obtained demonstrate that it is possible to obtain energy to sustain an autothermal pyrolysis process from these residues at operation temperatures above 500 °C. Residual biomass materials with high lignin content deliver gases with higher heating values (up to 23 MJ/m^3), higher yields of solids (ca. 58 %), and bio-oil with lower acid and higher phenolic content (up to 19.9%m/m.). Agricultural residues, especially hemp hurd, which contains lower lignin amount, produce chars with narrow microporosity, matching the requirements to selectively adsorb CO_2 from biogas and steam reforming streams, achieving CO_2/CH_4 selectivity values as high as 53.

List of abbreviations

A_{BET}	Specific surface area calculated by Brunauer, Emett, Teller method (m^2/g)	% m/m	Mass fraction (%)
AS	Almond shell	NDIR	Non dispersive infrared analyzer
AS-800	Char obtained from the pyrolysis of AS at 800 °C	NIST	National Institute of Standards and Technology
AST	American Science & Technology	NREL	National Renewable Energy Laboratory
BST	Bed Service Time (s)	OL	Organosolv Lignin
C	Outlet Concentration (mol/L)	OL-800	Char obtained from the pyrolysis of OL at 800 °C
C_0	Initial Concentration (mol/L)	OS	Olive Stone
ca.	Circa	OS-800	Char obtained from the pyrolysis of OS at 800 °C
DTG	Derivative Thermogravimetric analysis	p	Partial pressure
E_0	Adsorption Characteristic Energy (kJ/mol)	PSD	Pore size distribution
EBC	European Biochar Certificate	Q	Total gas flow rate (L/s STP)
EIHA	European Industrial Hemp Association	q_{BST}	Total amount of CO_2 adsorbed at BST (mmol $_{CO_2}$/g_{char})
EU	European Union	q_{CO_2}	Total amount of CO_2 adsorbed by char (mmol $_{CO_2}$/g_{char})
FC	Fixed Carbon	S_{CO_2}	Selectivity of CO_2 adsorption
GC/MS	Gas Chromatography coupled Mass Spectrometry	STP	Standard Temperature and Pressure
HH	Hemp Hurd	TCD	Thermal conductivity detector
HH-800	Char obtained from the pyrolysis of HH at 800 °C	TGA	Thermogravimetric Analysis
HHV	Higher Heating Value (MJ/kg)	VM	Volatile matter

(*continued on next column*)

(*continued*)

(*continued on next page*)

This article is part of a special issue entitled: Rafael Bilbao published in Biomass and Bioenergy.

* Corresponding author. Universidad de Málaga, Andalucía Tech., Departamento de Ingeniería Química, Escuela de Ingenierías Industriales, Campus de Teatinos s/n, 29010, Málaga, Spain.

E-mail address: mirasol@uma.es (J. Rodríguez-Mirasol).

https://doi.org/10.1016/j.biombioe.2025.107676
Received 20 December 2024; Received in revised form 1 February 2025; Accepted 1 February 2025
Available online 19 February 2025

(*continued*)

i	i component	$V_{micro}^{N_2}$	Micropore volume calculated from the N_2 isotherm (cm^3/g)
IPR	Independent Parallel Reactions	$V_{micro}^{CO_2}$	Micropore volume calculated from the CO_2 isotherm (cm^3/g)
IUPAC	International Union of Pure and Applied Chemistry	W	Mass of adsorbent in the adsorption column (g)
KL	Kraft Lignin	XRF	X-Ray Fluorescence
KL-800	Char obtained from the pyrolysis of KL at 800 °C	η	Adsorption column efficiency (%)
$L_0^{CO_2}$	Average micropore size (nm)	2D-NLDFT	2D-Non local Density Functional Theory
LHV	Lower Heating Value (MJ/Nm^3)	MSPs	minimum selling prices

1. Introduction

Pyrolysis of residual agricultural biomass feedstocks stands out as a sustainable thermochemical process to produce bioenergy and renewable products characterized by a net zero CO_2 emission. Pyrolysis of residual biomass generates three main products: a solid fraction with a high carbon content, known as biochar; condensable gases or liquids, usually referred as bio-oil; and non-condensable gases (bio-gas), such as CO, CO_2, CH_4, H_2, and short-chain hydrocarbons [1]. To achieve full sustainability of the process, integral valorization of all the products must be attained. In this sense, conventional uses of bio-char as energy source or as adsorbent have been recently expanded [2–4], and now includes soil amend and even carbon storage, due to its ability to fix carbon, allowing to generate value as carbon credit [5–7].The new European Union (EU) industrial carbon management laws underscore the significance of bio-char as an effective carbon sink, contributing to the reduction of atmospheric carbon dioxide levels [8]. Beyond its carbon sequestration potential, biochar also serves as an excellent soil amendment, improving soil fertility, water retention, and microbial activity. To align with these benefits and ensure environmental safety, compliance with the European Biochar Certificate (EBC) is essential [9]. The EBC mandates stringent criteria for biochar, including specific thresholds for carbon and hydrogen content, limited volatile matter, and the absence of pollutants like heavy metals and polycyclic aromatic hydrocarbons.

On the other hand, the bio-oil can be a valuable source of energy and value-added products, such as anhydrosugars, furans and/or phenolic compounds [10,11], whereas the gas is usually envisaged for obtaining the energy needed for the sustainable operation of the pyrolysis process. However, the heating value of pyrolysis gas is severely hindered by the presence of carbon dioxide. CO_2 removal by adsorption process is becoming more attractive due to the lower energy and size demands. The use of chars derived from biomass residues as adsorbents is of great interest because of their high thermal and chemical stability, as well as their environmental and economic advantages. Previously, the removal of CO2 from different product streams, using activated carbons, zeolites and bio-chars, has been studied in the literature [2,12]. The extensive scientific literature available on this topic has established through thermodynamic analyses that the ability to adsorb CO_2 is proportional to the volume of narrow micropores. However, the specific characteristics required for an adsorbent to selectively remove CO_2 under dynamic conditions in a complex gas mixture are not yet clearly defined. This highlights the need for kinetic adsorption analyses using fixed-bed column experiments to properly assess the CO2 removal selectivity under transient conditions. In this sense, the separation of CO_2 from the pyrolysis gas by this adsorption process would increase its heating value, generating biogenic CO_2 that could be integrated into the production cycle, with interesting applications in the food and beverage industry, metal manufacturing, refrigeration, greenhouses, production of construction materials, generation of renewable chemicals and fuels, etc., reducing the dependence on fossil resources and promoting a circular carbon economy [13]. Therefore, using the biochar produced during the pyrolysis of a residual biomass feedstock to upgrade the pyrolysis gas would also enhance the sustainability of the pyrolysis process.

The proportion in which the solid, liquid and gas fractions are obtained depends to a large extent on the pyrolysis operating conditions (temperature, heating rate, residence time of the gases and solids inside the reactor) and also on the lignocellulosic composition of the biomass feedstock [14,15]. Professor Rafael Bilbao and his research group extensively studied the pyrolysis of lignocellulosic materials in the late 1980s and early 1990s, providing relevant conclusions on the influence that different operating conditions and the composition of the biomass has on the solid conversion, yield and pyrolysis products distribution and composition [16–19]. They also developed very useful kinetic models for the biomass solid conversion and gas formation in the thermal decomposition of different lignocellulosic materials, analyzing the influence of particle size, heating rate, thermal conductivity and reaction heat [20–25].

Pyrolysis conditions, such as low temperatures, slow heating rates and a long residence time promote repolymerization/recombination reactions, increasing the char yield [26,27]. In this sense, the potential application of the obtained char will rely on the chemical composition and the resulting porosity. High heating rates, moderate temperatures and short gas residence times, like those in fast pyrolysis, are of interest for producing liquids [11]. These features are likely associated not only with the process conditions, but also with the lignocellulosic, elemental and/or proximate composition of the biomass. High contents of holocellulose promotes the formation of volatiles compounds, which will favor the production of bio-oil and gas fractions. In contrast, lignin leads to a higher char yield during pyrolysis [28–31]. Deoxygenation of holocellulose seems to take place at low pyrolysis temperatures through dehydration reactions, while decarbonylation and decarboxylation are usually the main routes of decomposition of lignin at higher pyrolysis temperatures [32]. The distribution of these components varies among plants. In general, herbaceous plants show a higher content of holocellulose (hemicellulose and cellulose), while woody plants are characterized by a higher lignin content [33]. To enable the sustainable operation of pyrolysis processes by full integral valorization of all the obtained fractions, it is necessary to survey and mobilize underutilized agricultural residues, and to study and establish the relationship between agricultural feedstocks of different lignocellulosic composition, with the distribution and characteristics of the pyrolysis products [28,34,35].

Bearing this goal in mind, the pyrolysis of five biomass wastes of different origin and lignocellulosic composition (hemp hurd (HH), olive stones (OS), almond shells (AS), kraft lignin (KL), and organosolv lignin (OL)) have been studied under different operating conditions to analyze in detail the different products obtained. Industrial hemp (Cannabis Sativa L.) is an herbaceous plant worldwide cultivated for commercial purposes [36]. In addition, hemp is considered a highly efficient crop in CO_2 sequestration [36–38], showing a fast grow rate without needing insecticides or chemical treatments, which allows to absorb up to 13 tons of CO_2 per hectare harvested [39]. HH, which represents 70–80 % of the plant, could be considered as a lignocellulosic biomass of great industrial and economic interest [38]. The European Industrial Hemp Association's (EIHA) estimates that 50 000 ha were dedicated to grow hemp in the EU during 2018, reflecting a 70 % increase from 2013, the largest producers being France, Italy and The Netherlands [39]. OS, a woody biomass waste, is the main solid residue of the olive oil industry. Around 4 million tons of OS are generated annually in the world, primarily in the Mediterranean region [40], being currently managed as biofuel for the generation of electrical and thermal energy owing to its heating value of *ca.* 18 MJ/kg. AS constitutes another highly available woody biomass. Shells constitutes around 50 % of the total mass of the almond fruit, and the global almond production reached a total volume of 1.5 million metric tons in 2023, with United States, Australia and

Spain contributing 76, 10 and 4 % of the total, respectively [41].

Lignin is the main sub-product of the pulp industry, with an annual worldwide production of *ca.* 50 million tons, with 98–99 % being currently burned in the plant to produce energy [42]. However, the fraction recovered from black liquors for commercial purposes is increasing, as it is also regarded as a sustainable feedstock for the production of aromatics, chemicals, materials and bioenergy [43]. The Kraft process is the most implemented pulping process, using sodium hydroxide and sulfide to depolymerize lignin, generating soluble fragments and incorporating sulfur and inorganic elements into the composition of the product. Differently, Organosolv process involves the use of water and an organic solvent, such as butanol, ethanol, or acetone, to carry out lignin extraction, obtaining a technical lignin free of inorganic content and sulfur. Organosolv processes are envisaged for the separation of biopolymers in second generation lignocellulosic biorefineries, where the valorization of lignin into chemicals, materials and energy could potentially improve the overall profitability of the plant.

This work reports a detailed characterization of all the fractions obtained during the slow pyrolysis of five different agricultural wastes, at temperatures from 400 to 800 °C. The stablished correlation between the lignocellulosic biomass composition and the properties of each of the pyrolysis products obtained (bio-oil, biochar and gases) in relation to their potential applications (in addition to the distribution of pyrolysis products and yields) represents the main novelty of this work. In particular, the study of hemp hurds, a biomass residue that has received less attention in this context, is highlighted. Moreover, the results obtained have been compared with other biomass with different lignocellulosic compositions, thus stressing the relevance and potential of this non-conventional feedstock in applications related to the valorization of biomass residues. The characterization not only reports chemical composition and energy content including the evaluation of chars as carbon sinks and as novel CO_2 adsorbents in different gaseous streams, such as biogas, reforming streams and gas fraction from pyrolysis, which would allow full integration of the products into the pyrolysis process. The complete characterization of the products not only allow to study the effect of the biomass waste biopolymer composition on the pyrolysis products distribution but also enables to identify the relationships between the properties of feedstocks and the most viable biomass valorization pathways (i.e. solid *vs* liquid *vs* energy production).

2. Materials and methods

2.1. Materials preparation and characterization

Five different lignocellulosic biomass residues were studied, hemp hurds (HH) provided by Alsativa (Sociedad Cooperativa Agraria Andaluza del Cáñamo, Pórtugos, Granada), olive stones (OS) supplied by Sociedad Cooperativa Andaluza Olivarera y Frutera San Isidro (Periana, Málaga), almond shells (AS) from Cerro Tumbajarro (Aguilar de la Frontera, Córdoba), organosolv lignin (OL), supplied by American Science and Technology Corp., AST (now Attis Innovations), and Kraft lignin (KL) produced by Westvaco Chemical Division. The different biomass residues were dried at 105 °C overnight and, subsequently, crushed and sieved between 300 and 400 μm.

The proximate analysis (i.e., moisture, volatile matter, fixed carbon and ash contents) was studied through thermogravimetric analysis (TGA) experiments in thermobalance (NEXTA STA300), according to ASTM E1131-08. The ultimate analysis was recorded in a TruSpec micro CHNSO (Leco) analyzer, being the mass fraction of oxygen determined by difference. The inorganic composition of biomass was calculated in a wavelength dispersive X-Ray spectrometer at 60 kV (ARL ADVANTXP) by X-Ray Fluorescence (XRF).

The bulk density of the feedstocks was analyzed according to ASTM D 2854-09 and the composition of the biopolymers was obtained by TAPPI methodology (Extractives: TAPPI 264, Holocellulose: Rowell et all. and Lignin: TAPPI 222) [44].

2.2. Pyrolysis experiments

The slow pyrolysis of different biomass residues was carried out in a stainless-steel (SS) fixed bed reactor (inner diameter: 2 cm; length of isothermal zone: 4 cm, sample holder: SS316L disk filter). In a typical experiment, 3 g of dry biomass were loaded into the reactor and heated at different temperatures (400, 500, 600 and 800 °C, pressure: 1 atm, heating rate: 10 °C/min, holding time: 1 h) by an electric furnace (Hobersal TR-1), under N_2 flow (150 cm^3 STP/min). The bed temperature was monitored with a thermocouple (type K). Once the experiment was finished, the reactor was cooled down under inert atmosphere and the solid fraction was recovered from the reactor (Fig. S1).

At the reactor outlet, different custom glass condensers were placed to collect the bio-oil. The first condenser was kept at room temperature, while the other ones were set at −10 °C using a chiller (minichiller 300 OLE, Julabo). A cotton filter and a candle stainless steel filter (pore size: 15 μm) were in-line connected at the exit of the second condenser to provide a clean gas stream. The composition of the non-condensable gas stream was monitored combining the results of on-line continuous gas analyzers with the Gas Chromatography-Mass Spectrometry (GC/MS) analysis from the gas collected in a Tedlar sampling bag (see section 2.4 for more details). The yields to the solid and liquid fractions were calculated by weighing the char and the bio-oils collected from the condensing systems and dividing each value, respectively, by the starting mass of dried biomass. The non-condensable gas fraction was obtained by difference.

2.3. Analysis of the condensable gases (bio-oil)

The collected bio-oil was stored at −20 °C inside a stopped vial. A 50 μL aliquot of bio-oil was recovered for analysis by Gas Chromatography-Mass Spectrometry (GC/MS) analysis using a 7000D GC/MS Triple Quad (Agilent Technologies, USA). The GC/MS system incorporates an Agilent HP-5ms column (30 m × 0.250 mm x 0.25 μm). The temperature program used consisted of an initial step of 60 °C for 10 min, followed by a temperature increase up to 250 °C at a heating rate of 10 °C/min, with a holding time of 20 min. Compound identification was carried out with NIST MS Search 2.0 mass spectral library, and quantification was achieved following the laboratory analytical procedure from NREL [45]. The water content of the bio-oil was determined by Karl Fischer titration using a KF V20 (Mettler Toledo, USA).

2.4. Analysis of the non-condensable gases

The evolution of the main gases, CO, CO_2, CH_4 and H_2, were continuously registered with TCD and non-dispersive infrared gas analyzers (Ultramat 23 and SIPROCESS GA700 systems, Siemens, Germany). The composition in other non-condensable gases (C2-C4 hydrocarbons) was established from the gas collected using a 3 L Tedlar gas sampling bag every 20 min and analyzed in a PerkinElmer Autosystem gas chromatograph (GC) equipped with a Hayesep Q (80/100) column (isothermal step of 120 °C, for 20 min) and FID detector. The identification and quantification of C1-C4 paraffins and olefins were carried out through external calibration using a standard commercial gas mixture with Helium provided by Linde Gas España S.A.U. The lower heating value (LHV, MJ/Nm^3) of the non-condensable gases was calculated by the following equation (1).

$$LHV = 0.126 \cdot CO + 0.108 \cdot H_2 + 0.357 \cdot CH_4 + 0.640 \cdot C_2H_6 + 0.911 \cdot C_3H_8 + 0.590 \cdot C_2H_4 + 0.859 \cdot C_3H_6 \quad (1)$$

where H_2, CH_4, C_2H_6, C_3H_8, C_2H_4 and C_3H_6 represent the concentration of the different gases in volumetric %.

2.5. Analysis of the solid fraction

The chemical composition of the solid fraction was studied by ultimate analysis in a TruSpec micro CHNSO analyzer (Leco) to determine the mass fractions of carbon (C), hydrogen (H), nitrogen (N) and sulfur (S); the oxygen content (O) was calculated by difference (considering the ash content to the CHNS composition). The inorganic composition and proximate analyses of the chars were established as reported in **section 2.1** for the biomass feedstocks. The higher heating values (HHV, MJ/kg, dry basis) were calculated according to Cordero et al. (2) equation [46,47].

$$HHV = 0.354 \cdot FC + 0.171 \cdot VM \quad (2)$$

where FC and VM represent the fixed carbon and volatile matter content, respectively, indicated in the proximate analysis, and C, H, O and S the carbon, hydrogen, oxygen and sulfur content, respectively, measured in the ultimate analysis. The porosity of the chars was studied by N_2 adsorption-desorption and CO_2 adsorption isotherms at −196 °C and 0 °C, respectively, using an ASAP 2020 equipment (Micromeritics Instruments Corporation). Previously to every analysis, the samples were outgassed at 150 °C during 8 h. The BET surface area, A_{BET}, and the micropore volumes derived from N_2 and CO_2 adsorption isotherms, $V_{micro}^{N_2}$ and $V_{micro}^{CO_2}$, respectively, were determined in accordance with the IUPAC recommendations [48]. The pore size distribution (PSD) was calculated from the CO_2 adsorption isotherm using the 2D-NLDFT heterogenous surface model, as implemented in SAIEUS Software (Micromeritics) [49]. The average micropore size (L_0) was determined using the equation of Stoeckli et al. (3), applicable for pore sizes in the range of $0.4 < L_0 < 2$ nm, with a characteristic energy between 20 and 42 kJ/mol [50,51].

$$E_o = \left(\frac{10.8}{L_0}\right) + 11.4 \quad (3)$$

where E_o (kJ/mol) is the characteristic energy.

2.5.1. Gas separation study

The chars obtained during the pyrolysis were tested as possible CO_2 low-cost adsorbents for the upgrading of three different gaseous streams, namely: i) pyrolysis gas (42 % CO_2, 32 % CO, 16 % H_2 and 10 % CH_4); ii) simulated biogas (50–70 % CH_4 and 50-30 % CO_2); iii) and steam reforming gas stream (25–75 % H_2 and 75-25 % CO_2). Argon (99.999 %) was used as an inert carrier and as purge agent. All cylinder gases (CH_4, 95.00 %, CO, 99.99 %, CO_2 99.99 %, H_2 99.99 %) were provided by Linde Gas España S.A.U. A custom-made gas mixing setup equipped with 4 mass flow controllers (5850S, Brooks, The Netherlands) was used to achieve the different compositions of the gas streams. The composition of the gas stream at the column outlet was continuously monitored using NDIR and TCD detectors (Ultramat 23 and SIPROCESS GA700systems, Siemens, Germany).

Adsorption experiments were carried out in a jacketed, glass fixed-bed column (internal diameter: 0.4 cm), at 25 °C and atmospheric pressure, using a gas flow rate of 50 cm^3 STP/min. The dead volume of the adsorbing system was determined using a pure CO_2 stream as a tracer, obtaining a result of 34 cm^3. In a typical run, 1.00 g of dried char is loaded into the column and purged for 1 h with argon at 100 °C before starting the adsorption experiments. Once saturation of the adsorbent was reached (the concentration at the adsorbent bed outlet was equal to that of the gas inlet), the desorption step was performed at same adsorption conditions by replacing the gas inlet with a pure Argon stream. Desorption process was finished when CO_2 was not detected in the outlet stream (<2 ppmv). Quantification of the different adsorbed and desorbed gases (CO_2, CO, H_2 and CH_4) was determined from the breakthrough profiles. As a result, the bed service time (BST), and column efficiency were calculated. The BST (s) was defined as the duration required for the outflow concentration to achieve 10 % of the initial flow concentration ($C/C_0 = 0.1$). The column efficiency (%) was calculated according to equation (4).

$$Column\ efficiency\ (\%) = \frac{q_{BST}}{q_{CO_2}} \cdot 100 \quad (4)$$

In it, q_{CO_2} is the total amount of CO_2 adsorbed by the char ($mmol_{CO_2}/g_{char}$) at saturation time, t_s (s), and q_{BST} corresponds to the amount of CO_2 adsorbed at the BST ($mmol_{CO2}/g_{char}$) [12],:

$$q_{CO_2} = \frac{C_0 \cdot Q}{W} \cdot \int_0^{t_s} \left(1 - \frac{C}{C_0}\right) \cdot dt \quad (5)$$

$$q_{BST} = \frac{C_0 \cdot Q}{W} \cdot \int_0^{BST} \left(1 - \frac{C}{C_0}\right) \cdot dt \quad (6)$$

Where C_0 is the CO_2 inlet concentration (mol/L), Q is the total gas flow rate (L/s STP), W is the mass of adsorbent used in the fixed bed (g), and C is the CO_2 concentration (mol/L) registered at the column outlet during the adsorption experiment.

The kinetic selectivity analysis of CO_2 in binary and quaternary streams has been calculated according to equation (7).

$$S_{\frac{CO_2}{i}} = \frac{\frac{q_{CO_2}}{q_i}}{\frac{p_{CO_2}}{p_i}} \quad (7)$$

where i is the component, q the total adsorbed amount, and p_i is the partial pressure of i component [52].

3. Results and discussion

3.1. Characterization of the feedstock

Table 1 shows the main properties of the lignocellulosic biomass residues. HH reveals the moisture (M), higher volatile matter content (VM), followed by OS, AS, OL, and KL. High VM content is expected to improve the gas and liquid yield during the pyrolysis process [53,54]. A linear trend between holocellulose and extractives and VM is observed, Table 1. Similarly, the fixed carbon content (FC) is clearly related to the lignin content of the feedstocks. Notably, the five biomass residues contain low amounts of ash (<3 % m/m). KL shows the highest ash content, followed by AS and HH, while OS and OL are almost inorganic matter free. Regarding the ultimate analysis, HH, OS, and AS showed similar results, with C/O ratios close to 1 due to their high holocellulose content. In contrast, the two lignins presented a higher content of C and lower levels of O than the other biomass, since they show an aromatic character structure, and the presence of N and S heteroatoms, derived from their extraction process.

As for the heating values (HHV, Table 1), the lower HHV value is attained by the HH, while the technical lignins shows the highest energy content, given the larger FC content in lignins. Apart from the energy content, bulk density is a critical parameter for the economic feasibility of long-range transportation of biomass feedstocks used as biofuel. The use of HH as biofuel can be ruled out due to the low HHV and bulk density. This low volumetric energy value increases the interest in using HH as on site pyrolysis feedstock, which can increase the specific energy density of the solid and liquid fractions. Meanwhile, OL shows the highest bulk density and HHV, enabling its potential use as biofuel. OS, AS and KL shows mid-range values, supporting their current use as bioenergy source without ruling out their potential use as pyrolysis feedstocks. It is worth noting that less dense biomass feedstock can be pelletized, which significantly improves their bulk density. This process can be achieved at a relatively low energy and fiscal cost.

The inorganic composition has been determined by XRF, Table S1, finding elements such as K and Ca as the main compounds in the agricultural wastes (HH, OS and AS). According to different studies, the presence of alkali-metal elements as K can promote the thermal

Table 1
Physiochemical properties of different lignocellulosic biomass residues.

		HH	OS	AS	OL	KL
Proximate analysis (%m/m.)[a]	**M**	5.2 ± 0.1	5.7 ± 0.1	2.5 ± 0.1	1.3 ± 0.1	0.4 ± 0.1
	VM	84.3 ± 0.8	79.6 ± 0.8	78.7 ± 0.8	63.1 ± 0.6	55.6 ± 0.6
	FC	14.3 ± 0.1	19.9 ± 0.2	20.0 ± 0.2	36.9 ± 0.4	41.7 ± 0.4
	Ash	1.4 ± 0.1	0.5 ± 0.1	1.5 ± 0.1	–	2.7 ± 0.1
Ultimate analysis (%m/m.)[b]	**C**	48.6 ± 0.6	48.3 ± 0.6	49.0 ± 0.6	64.8 ± 0.8	66.0 ± 0.9
	H	5.9 ± 0.1	6.1 ± 0.1	6.3 ± 0.1	6.7 ± 0.1	6.3 ± 0.1
	N	0.2 ± 0.1	0.2 ± 0.1	0.2 ± 0.1	2.5 ± 0.1	0.8 ± 0.1
	S	–	–	–	0.3 ± 0.1	1.3 ± 0.1
	O[c]	45.3 ± 0.2	45.4 ± 0.2	44.5 ± 0.2	25.8 ± 0.1	25.6 ± 0.1
HHV (MJ/kg)[d]		19.5 ± 0.1	20.6 ± 0.1	20.5 ± 0.1	23.9 ± 0.1	24.3 ± 0.1
Bulk density (g/cm³)		0.123 ± 0.001	0.481 ± 0.001	0.581 ± 0.001	0.714 ± 0.001	0.471 ± 0.001
Biopolymers composition (%m/m.)	**Holocellulose**	69.6 ± 0.8	65.1 ± 0.8	54.3 ± 0.7	18.0 ± 0.2	3.0 ± 0.1
	Lignin	21.0 ± 0.3	32.1 ± 0.4	36.3 ± 0.4	82.0 ± 1.0	97.0 ± 1.2
	Extractives	9.4 ± 0.1	2.8 ± 0.4	9.4 ± 0.1	–	–

[a] Dry basis.
[b] Dry ash free basis.
[c] Calculated by difference.
[d] Calculated by Cordero et al. equation from Ref. [47].

degradation of hemicellulose and cellulose, while alkaline-earth elements, as Ca, can have an inhibition impact on the hemicellulose degradation [55–57]. In the case of KL, the presence of Na and K has been attributed to the sodium salts used during the lignin depolymerization process.

3.1.1. Thermal decomposition analysis

The thermal degradation of the different lignocellulosic residues has been analyzed by the determination of mass loss with respect to temperature by non-isothermal thermogravimetric analysis under an inert atmosphere, Fig. 1. These experiments allow to study the pyrolysis behaviors of the main components of biomass (hemicellulose, cellulose and lignin) and select the temperature for the pyrolysis process [28].

The main thermal degradation for the three agricultural wastes (HH, OS and AS) takes place in a temperature range between 200 and 500 °C, each of them showing two peaks in the DTG profile (black lines in Fig. 1). The first peak (200–320 °C) is associated with the degradation of hemicellulose, while the second peak (320–380 °C) is connected to the degradation of cellulose. Finally, a third, ill-defined shoulder appears between 400 and 500 °C, which is traditionally ascribed to the lignin degradation [34,58,59]. The latter peak is more pronounced in the OS and AS due to their larger lignin contents, Table 1. Thermal degradation of lignin is a heterogeneous process that takes place between 200 and 900 °C due to the amorphous structure of lignin and the presence of chemical domains, functional groups and bonds of different strength [60]. Consequently, a broad DTG peak is observed in the mentioned temperature range for OL and KL. The presence of a small shoulder associated with the thermal degradation of hemicellulose, which partially precipitates during lignin isolation in the pulp industry, can be observed at 200–400 °C, being more pronounced in OL. Beyond 600 °C, only minor mass losses are registered for all samples, being mainly connected to the reactions associated to the carbonization process of char, such as aromatic condensation, dehydroxylation and decarbonylation.

Based on the data obtained by DTG, the biopolymer composition of each biomass can be determined. This analysis was carried out by the deconvolution of the different components of the biomass at the mentioned temperatures, using a first order independent parallel reactions (IPR) kinetic model (see supplementary file for equations details **(S1)** and **(S2)**) [61]. The results obtained indicate reasonable agreements between the holocellulose and lignin compositions determined following the TAPPI norms (Table 1) and the IPR kinetic modelling of the TGs (deviations lower than 11 % over the total holocellulose content and <4 % for lignin content) (Table S2) [62,63]. Interestingly, cellulose content was found to be higher for HH (54.4 % cellulose), while OS and AS showed lower, yet similar, values (38.6 % and 41.5 % cellulose, respectively). These contents are in agreement with those reported for HH by Rowell et al. [44], and for OS and AS elsewhere [64,65].

This study of non-isothermal decomposition of the different residual biomasses selected allows to select the operating temperatures in the pyrolysis process, which is the factor having the highest impact on obtaining the desired products, both in terms of yield and the composition of the different fractions [34]. According to the results in Fig. 1, a wide range of temperatures (400, 500, 600 and 800 °C) has been selected to evaluate the influence of temperature in the pyrolysis process on yields and composition of the products, in order to achieve i) hemicellulose decomposition ii) holocellulose decomposition, iii) main decomposition of lignin, and iv) promoted carbonization of the char.

3.2. Pyrolysis yields

In accordance with the previous findings, the pyrolysis yields from the different biomass (HH, OS, AS, OL and KL) were determined at pyrolysis temperatures of 400, 500, 600 and 800 °C and compiled in Fig. 2. The results confirm that, for all biomass, the solid fraction decreases with increasing temperature, while the yields to the liquid and gas fractions increase due to the higher contribution of devolatilization, depolymerization and cracking reactions at higher temperatures [66]. Regarding OS, a decrease in the bio-oil yield is observed above 500 °C. This behavior can be attributed to the fact that condensable compounds that are produced during the holding time at 500 °C can suffer secondary reactions of decomposition at higher temperatures, resulting in a reduction in the yield of the bio-oil fraction and an increase in the yield of the gas fraction. Differently, AS shows a similar bio-oil yield at higher temperatures, probably as a result of the higher stability of the condensable compounds generated from this sample. Thus, the liquid yield values at 800 °C, are 21, 30 and 31 %m/m. for OS, AS and OL, respectively (Fig. 2f)) [28]. In line with these results, Agnihotri et al. studied the effect of the temperature variation during a biomass pyrolysis process. These authors observed that the optimum temperature for bio-oil production was achieved at around 550 °C, above this temperature the bio-oil yield decreases, whereas at temperatures above 600 °C the gas yields predominated, due to the previously mentioned secondary reactions. These results support the data obtained in the distribution of products generated during the pyrolysis process [15].

However, different trends can be observed between samples, which

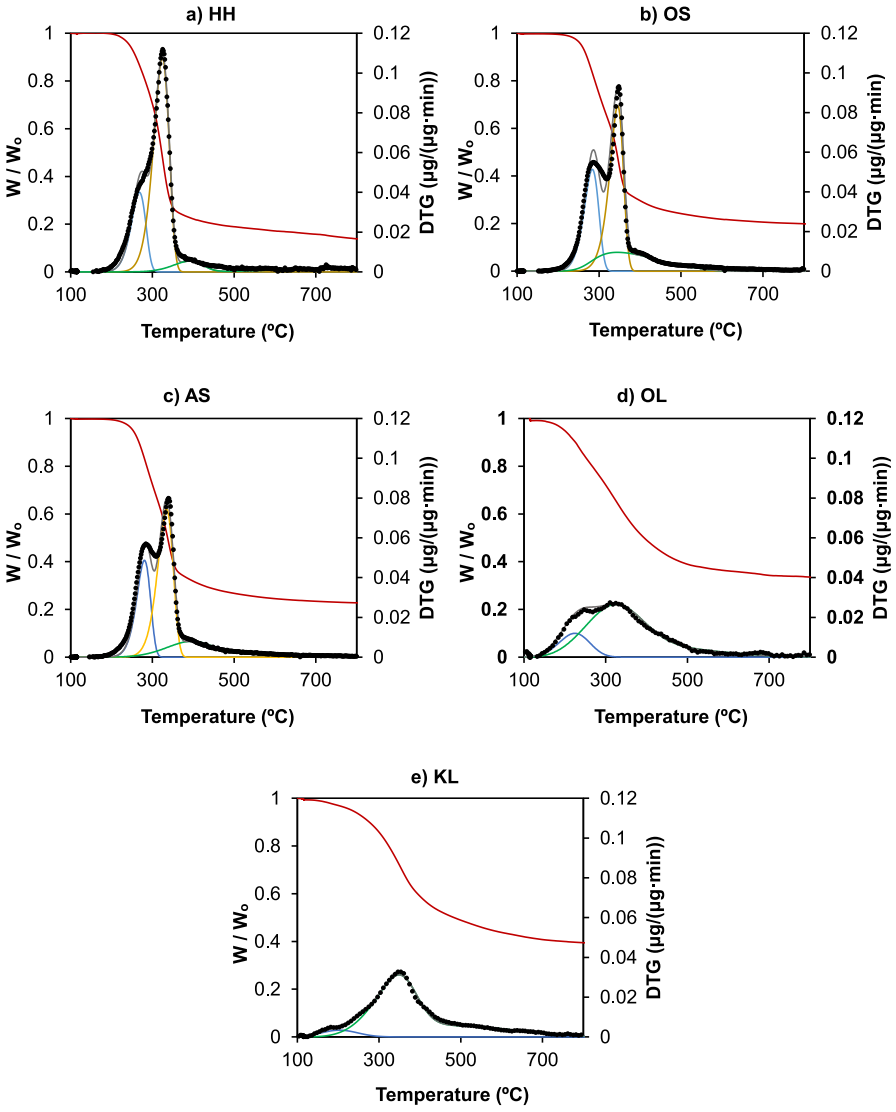

Fig. 1. Mass loss during non-isothermal TGA of biomass (red line), DTG (black dotted) and DTGs deconvolution corresponding to hemicellulose (blue line), cellulose (yellow line) and lignin (green line) curves, obtained at 800 °C, using a heating rate of 10 °C/min and a gas flow of 150 cm3 STP/min for a) HH, b) OS, c) AS, d) OL and e) KL. (For interpretation of the references to colour in this figure legend, the reader is referred to the Web version of this article.)

can be explained in terms of the different lignocellulosic composition and the presence of inorganic matter. It was found that: i) the higher the lignin content, the higher the formation of char and the lower the generation of non-condensable gases, for all the explored pyrolysis temperatures; ii) at 400 °C, the holocellulose content correlates well with the formed liquid fraction; iii) the optimum temperature for promoting the liquid-fraction is 500 °C for the biomass residues with higher holocellulose content; iv) the optimal temperature for liquid formation in technical lignins is over 600 °C, with KL achieving the highest liquid yield at 800 °C.

A final comparison between the pyrolysis yields at the highest pyrolysis temperature (Fig. 2f) reveals that the liquid fraction presents the highest yield for HH, with 59 % m/m., followed by OS, AS, KL and finally OL, that presents only a value of 36 % m/m. These results show a good agreement with the VM and holocellulose content, Table 1. As for the gas fraction, the highest yield is for OL with 31 % m/m. However, the high lignin content present in KL makes this biomass present the highest char yield with 42 % m/m. Interestingly, the higher lignin content of AS (36.3 % m/m.) does not deliver an increase in pyrolysis yield of the solid fraction, which shows a value even lower than that observed for OS (32.1 % m/m). This feature is probably linked to the larger presence of potassium and calcium species in AS, which catalyze the cracking reactions of volatiles and the gasification of the solid at 800 °C, promoting the formation of gas and decreasing the solid yield value below that obtained for OS under the same pyrolysis temperature [29,31]. This result illustrates the relevance of the inorganic content, and specifically of alkali elements, in the pyrolysis process.

3.3. *Condensable vapors fraction (bio-oil)*

Condensable vapors fraction has been collected in a condenser system located at the reactor outlet. The water and organic contents and the distribution of organic compounds are detailed in Table 2.

Focusing on the water content, the results obtained for pyrolysis of HH at different temperatures indicate that most water is generated during dehydration and condensation reactions at temperatures lower than 400 °C, as the water content barely changes from 400 to 500 °C [35]. This value slightly increases at temperatures above 500 °C, where the additional release of water could be explained by condensation reactions involving hydroxyl and phenols groups of lignin [35]. Regarding the organic fraction, most organic compounds are formed at 400 °C, probably because of the full decomposition of hemicellulose and partial

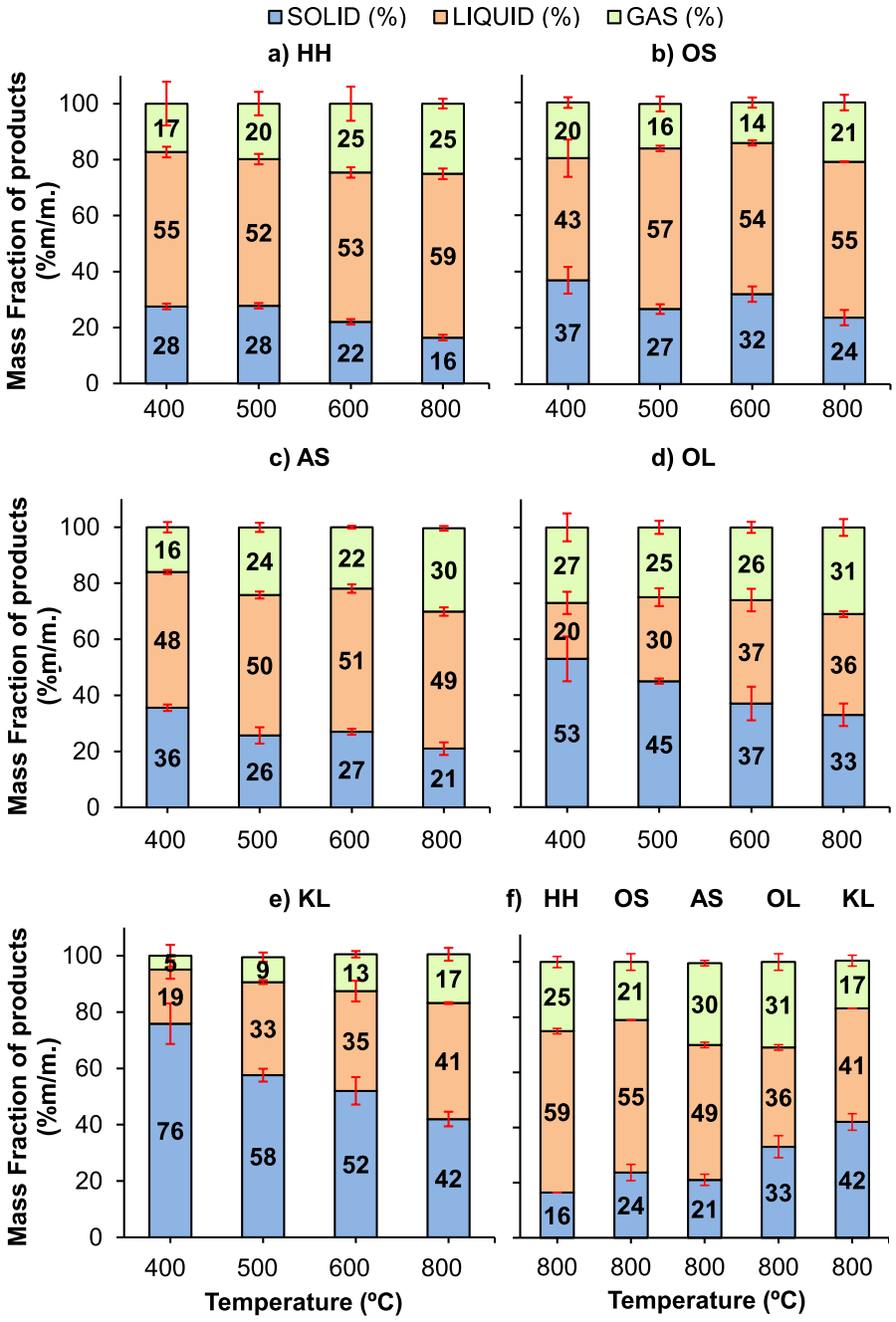

Fig. 2. Different mass fraction of products (% m/m.) values for the pyrolysis of a) HH, b) OS, c) AS, d) OL and e) KL at different temperatures, and f) comparison of the mass fraction of products from pyrolysis of different residual biomass at 800 °C.

Table 2
Quantitative analysis of water content and organic fraction in bio-oil, and product distribution of the bio-oil fraction from the pyrolysis of HH at different temperatures, and of OS, AS, OL and KL at 800 °C.

Sample	T (°C)	Water Content (%m/m.)	Organic Fraction (%m/m.)	Product distribution of bio-oil (% m/m.)			
				Acids	Furans/Ketones	Aromatics/Phenols	Alcohols/others
HH	400	17.0 ± 0.2	38.0 ± 0.4	6.4 ± 0.1	2.0 ± 0.1	6.1 ± 0.1	23.5 ± 1.0
	500	15.8 ± 0.2	36.6 ± 0.4	9.3 ± 0.1	3.5 ± 0.1	10.1 ± 0.1	13.6 ± 1.0
	600	17.8 ± 0.2	35.6 ± 0.4	12.9 ± 0.1	1.9 ± 0.1	7.2 ± 0.1	13.6 ± 1.0
	800	19.3 ± 0.2	39.2 ± 0.4	15.3 ± 0.1	1.8 ± 0.1	10.3 ± 0.1	11.8 ± 1.0
OS	800	15.7 ± 0.2	39.6 ± 0.4	13.9 ± 0.1	1.9 ± 0.1	10.6 ± 0.1	13.2 ± 1.0
AS	800	29.0 ± 0.3	20.0 ± 0.2	6.3 ± 0.1	1.0 ± 0.1	12.5 ± 0.1	0.2 ± 1.0
OL	800	21.2 ± 0.2	14.8 ± 0.1	1.3 ± 0.1	0.2 ± 0.1	8.7 ± 0.1	4.3 ± 1.0
KL	800	5.2 ± 0.1	36.0 ± 0.4	0.6 ± 0.1	0.3 ± 0.1	19.9 ± 0.1	15.2 ± 1.0

degradation of cellulose. Only a minor increase is observed when temperature is raised from 500 to 800 °C, as the outcome of lignin degradation, forming oxygenated aromatics compounds.

Further comparison with the results obtained from the rest of feedstocks at 800 °C points out that the formation of organic chemicals seems to be related to the presence of holocellulose, since AS shows a lower yield to condensable organic species than OS and HH, Table 2. Pyrolysis of KL generates a highly viscous bio-oil with a low water content (5.2 %m/m.), while the liquid phase obtained from OL shows a higher proportion of water (21.2 %m/m.) and lower formation of organic compounds. Such differences are probably connected to their different average molecular masses, as recently determined by gel permeation chromatography [67]. The harsh conditions of the Kraft process deliver an intense fragmentation of the lignin polymer, achieving much lower molecular sizes and a more condensed structure than in the lignin isolated by the Organosolv process. When submitted to pyrolysis, the small lignin oligomers of the Kraft process are probably recovered as tars and oxygenated aromatics. Differently, the pyrolysis of the OL, which is richer in oxygen functional groups and preserves much higher molecular sizes, generates a higher formation of water (from the mentioned oxygen groups) and char (due to the higher molecular size of the backbone of the lignin polymer), suppressing the production of organic compounds (14.8 and 36.0 % m/m. of organic fractions for OL and KL, respectively).

The liquid fraction has been analyzed by GC-MS, and due to the diversity of compounds identified by this analysis (as shown in Tables S3, S4, S5, S6 and S7), the content of these compounds was quantified and classified into acids, furans, ketones and phenols, as shown in Table 2 [10]. Acetic acid stands out as the predominant compound (Table S3), being produced by the breakdown of the acetyl groups present in the hemicellulose structure. Furfural and 5-methyl-Furfural are the main chemicals identified and quantified on the furans/ketones group (Table S8). Guaiacol and creosol are the most abundant oxygenated aromatic compounds on the aromatic/phenol family, being found in large quantities in OL and KL bio-oils (Table S8), while methanol was the predominant alcohol. Note that the concentration of several highly volatile oxygenated compounds that are known to be formed during pyrolysis in large quantities, such as formaldehyde and acetaldehyde, could not be determined due to the limitations of GC-MS technique. Their unknown amounts are gathered along with alcohols under the "others" label.

Among the various precursors analyzed, the largest fraction of bio-oil (as can be seen in section 3.2) was obtained from HH. In addition, the bio-oil derived from lignin is more suitable, in terms of quality and considering the potential cost of the products. The bio-oil derived from HH pyrolysis at 400 °C was mainly composed of alcohols and other oxygenated aliphatic compounds, followed by aliphatic acids, phenols and finally furans and ketones in lower amounts. An increase in temperature also leads to the formation of acids, becoming the predominant group of compounds at 800 °C, and phenols, due to the degradation of lignin at higher temperatures [68,69]. Comparing the three agricultural precursors at 800 °C, it is possible to establish a relationship between the holocellulose content and the formation of acids, as the acid content followed the order HH > OS > AS. Furans were also detected in larger amounts in the samples with higher holocellulose content (HH, OS and AS), and are known to be produced during thermal decomposition of xylose, present in hemicellulose, facilitating the formation of furfural and its derivatives. The thermal decomposition of OL and KL is clearly different, and showed a high proportion of phenols, derived from the methoxy groups of the aromatic structure of lignin, and aromatics, compared to the other precursors, followed by alcohols, confirming that these compounds are mainly obtained from lignin devolatilization [28]. In the case of the pyrolysis of OL, butanol and some esters of this alcohol have been observed in the bio-oil. Butanol could have been used as a solvent in the Organosolv process to obtain this lignin and has been able to recombine with the remains of the lignin groups by fractionating and solubilizing. Nevertheless, both bio-oils derived from the lignin precursors present low acid content, confirmed by neutral pH values, compared to the other bio-oils derived from agricultural residual biomass, showing pH below 3, which proves the promising composition of these lignin-derived bio-oils to produce aromatics and biofuels via upgrading processes as hydrodeoxygenation [70].

3.4. Non-condensable gas fraction

The non-condensable gas fraction constitutes a valuable source of renewable energy. The characterization of this fraction shows that, for all the feedstocks, the main components are CO, CO_2, CH_4 and H_2, along with small amounts of light hydrocarbons (C_2-C_3). The gas composition is strongly linked with the lignocellulosic composition and the pyrolysis temperature, as seen in Fig. 3a, b, c, d and e.

A clear link can be stablished between the presence of holocellulose and a higher evolution of CO_2 at 400 °C, (Fig. 3a–d). At this pyrolysis temperature, the gas fraction is mainly composed by CO_2 and CO for the agricultural residues, with CO_2 being produced by the thermal degradation of carboxyl functional groups of hemicellulose [71], while CO is originated through the breaking of ether and carbonyl bonds [35]. On the other hand, pyrolysis of lignin is related to the evolution of gases with higher heating values, i.e., CH_4, formed by cracking reactions and elimination of methoxy groups, and H_2, although only minimal release of this gas is observed at 400 °C (Fig. 3d and e).

When temperature increases, CO and CO_2 evolution remains mostly unaltered, Fig. 3, since the main source of these gases (i.e. holocellulose) is already pyrolyzed at 400 °C, while additional formation of CH_4 is observed for AS, OS and HH, due to the thermal decomposition of cellulose and specially lignin (which is more stable when found in native form), increasing the methane content in the pyrolysis gas. Hydrogen evolution starts to rise at 600 °C and increases with temperature, being more relevant in lignin-rich feedstocks. At 800 °C, additional release of CO and CO_2 is observed, due to the decomposition of thermally stable functional groups, such as phenols, quinones and carbonyls [72], from the freshly formed char, and also as a consequence of the decomposition of alkaline carbonates (Table S1), which usually decomposes in the 600–800 °C temperature range. However, in addition to the release of CO and CO_2 a huge increase in hydrogen content is also observed at 800 °C, which becomes the dominant component of the gas phase in the pyrolysis of technical lignins. The aromatic condensation responsible of the growing of the carbon microcrystalline domains during carbonization [73] and the cracking of hydrocarbons contributes to the generation of H_2. In fact, C_2-C_3 aliphatic hydrocarbons are also observed in higher amounts in the composition of the pyrolysis gas of technical lignins [39,74]. In the case of HH, the presence of iron, Table S1, which is known to have catalytic activity for the high temperature water gas shift [75], seems to enhance the formation of hydrogen at low pyrolysis temperature range, compared to the others agricultural residual biomasses.

Regarding the quality of the gas fraction for hydrogen production or syngas generation, a straightforward relationship between the lignin content (Table 1) and the H_2/CO molar ratio can be established, reaching values of 4.5, 2.3, 1.2, 1.2 and 0.5 for OL, KL, HH, AS and OS, respectively, at a pyrolysis temperature of 800 °C. A LHV has been also derived for the gas fractions obtained at the different pyrolysis temperatures studied, from the gas composition, using the equation (1), obtaining values of 8, 10, 13 and 13 MJ/m^3 STP for HH; 10, 10, 13 and 16 MJ/m^3 STP for OS; 10, 9, 11 and 11 MJ/m^3 STP for AS; 22, 25, 22 and 19 MJ/m^3 STP for OL; and 21, 23, 21 and 16 MJ/m^3 STP for KL at 400, 500, 600 and 800 °C, respectively. For biomass having high holocellulose content, the heating value of the pyrolysis gas increases with temperature. However, the LHV achieves the highest value at 500 °C when lignin is used as feedstock.

In order to analyze the role of the biomass composition on the gas pyrolysis yields, Fig. 3f presents the mass gas distribution from pyrolysis of HH, OS, AS, OL and KL at 800 °C, showing that OL is the most suitable

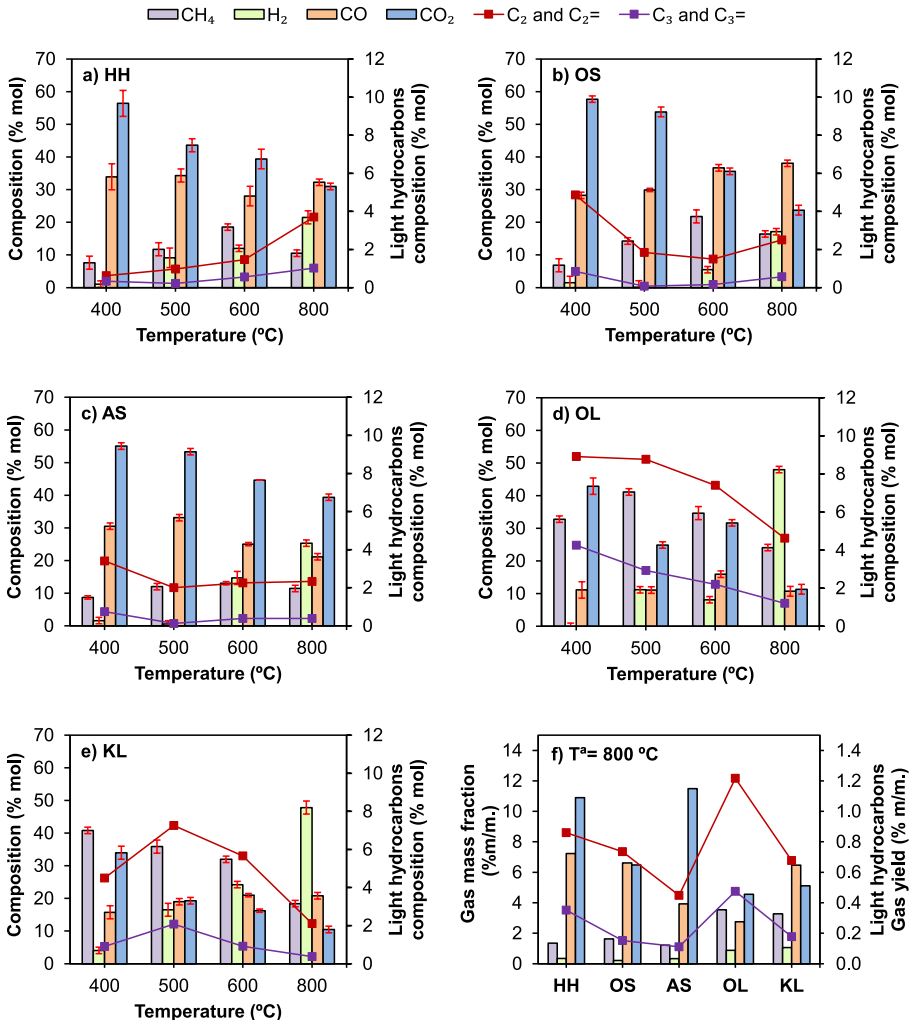

Fig. 3. Evolution of the molar composition of the pyrolysis gas fraction with temperature (400–800 °C) for a) HH, b) OS, c) AS, d) OL and e) KL. f) comparison of the gas gravimetric distribution for all the samples at 800 °C.

biomass to produce non-condensable gases with high HHV. CO and CO_2 are the main compounds for the three agrolignocellulosic residues due to their higher holocellulose content in these biomasses, while CH_4, H_2 and light hydrocarbons are observed in lower proportions. In contrast, a pyrolysis gas richer in CH_4 and H_2 is obtained from technical lignins. Combining the gas yields and the LHV it is possible to determine the energy content of the pyrolysis gas phase for the different biomasses, Table S9. The energy content increases with pyrolysis temperature, achieving values of 4.1, 3.8, 2.6, 4.4 and 5.6 MJ/$kg_{feedstock}$ for HH, OS, AS, OL and KL at 800 °C, respectively. Such an increase is due to the increasing contribution of CO, H_2, CH_4 and light hydrocarbons. The reported heat of reactions ranges from 0.21 to 0.44 MJ/kg for the pyrolysis of biomass residues [76]. When combined with the energy requirements to vaporize moisture and heat the feedstock can reach values as high as 2 MJ/kg [77], which can be covered by the energy content of the pyrolysis gases (Table S9) only for feedstocks analyzed in this study pyrolyzed at temperatures higher than 500 °C. For the rest of them, it would be advisable to derive energy obtained from the liquid or the solid product fractions to achieve sustainable operation of the pyrolysis processes.

3.5. Solid fraction

The proximate and ultimate analysis and the high heating value (HHV) of the bio-chars obtained from all the feedstocks at different pyrolysis temperatures have been gathered in Table 3.

The values of Table 3 reveal that the higher the pyrolysis temperature and the lignin content of the biomass residue the higher the fixed carbon content of the produced bio-char. Among the different biomass analyzed, KL was identified as the most suitable for bio-char production, as detailed in section 3.2. However, given the low BET surface area, which severely limit their performance as adsorbent for liquid phase applications, their potential uses are mainly restricted to gas-phase adsorption. The quality as adsorbent of the different biochars for these applications is highly reliant on the dynamic adsorption performance under different gaseous mixtures, which is studied in the next section.

Regarding the ultimate analysis of the chars derived from the agricultural residues, they present a high carbon (C) content, which increases with the pyrolysis temperature. In contrast, a decrease in the hydrogen (H) and oxygen (O) contents is observed due to decarboxylation, demethylation and condensation reactions, which occur with increasing temperature [35]. The nitrogen content is relatively low (≤0.3 %) and seems to be unaltered for all the temperatures and feedstock tested in this study, except for the biochar obtained from OL, which presents somewhat higher values, probably due to the presence of nitrogen compound in the Organosolv process for generating this lignin. In addition, no appreciable amounts of sulfur are observed for these samples. The low values of N and S content observed for this biochar decrease the potential NO_x and SO_2 emissions during the combustion of the chars in the case they were used to generate energy. Lignin-derived

Table 3
Physiochemical properties of bio-chars obtained from pyrolysis of HH, OS, AS, OL and KL at different temperatures.

Sample	Pyrolysis T (°C)	Proximate analysis (% m/m.)[a]			Ultimate analysis (% m/m.)[b]					HHV[d] (MJ/kg)	Bulk density
		VM	Ash	FC	C	H	N	S	O[c]		(kg/L)
HH	**400**	24.6 ± 0.2	5.1 ± 0.1	70.3 ± 0.7	76.6 ± 1.0	3.9 ± 0.1	0.3 ± 0.1	-[e]	19.2 ± 0.1	29.1 ± 0.1	0.21 ± 0.01
	500	21.3 ± 0.2	5.0 ± 0.1	73.7 ± 0.7	82.6 ± 1.1	3.3 ± 0.1	0.3 ± 0.1	-[e]	13.8 ± 0.1	29.8 ± 0.1	0.18 ± 0.01
	600	11.3 ± 0.1	6.4 ± 0.1	82.3 ± 0.8	83.7 ± 1.1	2.4 ± 0.1	0.3 ± 0.1	-[e]	13.6 ± 0.1	31.1 ± 0.1	0.23 ± 0.01
	800	6.9 ± 0.1	8.5 ± 0.1	84.6 ± 0.8	88.6 ± 1.2	1.0 ± 0.1	0.2 ± 0.1	-[e]	10.2 ± 0.1	31.2 ± 0.1	0.29 ± 0.01
OS	**400**	28.0 ± 0.3	1.4 ± 0.1	70.6 ± 0.7	71.1 ± 0.9	3.6 ± 0.1	0.3 ± 0.1	-[e]	25.0 ± 0.1	29.8 ± 0.1	0.80 ± 0.01
	500	22.7 ± 0.2	1.9 ± 0.1	75.4 ± 0.8	80.3 ± 1.0	3.0 ± 0.1	0.3 ± 0.1	-[e]	16.4 ± 0.1	30.6 ± 0.1	0.67 ± 0.01
	600	17.2 ± 0.2	2.5 ± 0.1	80.3 ± 0.8	85.4 ± 1.1	2.3 ± 0.1	0.3 ± 0.1	-[e]	12.0 ± 0.1	31.4 ± 0.1	0.66 ± 0.01
	800	12.4 ± 0.1	2.2 ± 0.1	85.4 ± 0.9	87.5 ± 1.1	0.8 ± 0.1	0.2 ± 0.1	-[e]	11.5 ± 0.1	32.4 ± 0.1	0.89 ± 0.01
AS	**400**	15.9 ± 0.2	4.2 ± 0.1	79.9 ± 0.8	75.7 ± 1.0	4.3 ± 0.1	0.5 ± 0.1	-[e]	19.5 ± 0.1	31.0 ± 0.1	0.67 ± 0.01
	500	13.4 ± 0.1	5.8 ± 0.1	80.8 ± 0.8	74.1 ± 1.0	2.7 ± 0.1	0.2 ± 0.1	-[e]	23.0 ± 0.1	31.0 ± 0.1	0.72 ± 0.01
	600	8.4 ± 0.1	5.5 ± 0.1	86.1 ± 0.9	87.9 ± 1.1	2.4 ± 0.1	0.3 ± 0.1	-[e]	9.4 ± 0.1	31.9 ± 0.1	0.70 ± 0.01
	800	4.5 ± 0.1	6.7 ± 0.1	88.8 ± 0.9	86.9 ± 1.1	1.0 ± 0.1	0.3 ± 0.1	-[e]	11.8 ± 0.1	32.2 ± 0.1	0.76 ± 0.01
OL	**400**	15.0 ± 0.2	0.5 ± 0.1	84.5 ± 0.8	86.1 ± 1.1	4.5 ± 0.1	3.4 ± 0.1	-[e]	6.0 ± 0.1	32.5 ± 0.1	0.60 ± 0.01
	500	9.2 ± 0.2	0.8 ± 0.1	90.0 ± 0.9	87.4 ± 1.1	3.3 ± 0.1	3.3 ± 0.1	-[e]	6.0 ± 0.1	33.5 ± 0.1	0.58 ± 0.01
	600	–	–	–	–	–	–	–	–	–	–
	800	3.4 ± 0.1	1.0 ± 0.1	95.6 ± 1.0	91.3 ± 1.2	1.0 ± 0.1	2.8 ± 0.1	-[e]	4.9 ± 0.1	34.5 ± 0.1	0.61 ± 0.01
KL	**400**	31.4 ± 0.3	3.5 ± 0.1	65.1 ± 0.7	73.4 ± 1.0	4.9 ± 0.1	0.4 ± 0.1	0.4 ± 0.1	20.9 ± 0.1	28.4 ± 0.1	0.60 ± 0.01
	500	28.0 ± 0.3	4.7 ± 0.1	67.3 ± 0.7	80.9 ± 1.1	3.2 ± 0.1	0.4 ± 0.1	0.8 ± 0.1	14.7 ± 0.1	28.6 ± 0.1	0.51 ± 0.01
	600	17.4 ± 0.2	5.3 ± 0.1	77.3 ± 0.8	87.9 ± 1.1	2.2 ± 0.1	0.5 ± 0.1	0.6 ± 0.1	8.8 ± 0.1	30.4 ± 0.1	0.50 ± 0.01
	800	6.5 ± 0.1	6.6 ± 0.1	86.9 ± 0.9	88.9 ± 1.2	0.9 ± 0.1	0.6 ± 0.1	0.6 ± 0.1	9.0 ± 0.1	31.9 ± 0.1	0.61 ± 0.01

[a] Dry basis.
[b] Dry ash free basis.
[c] Calculated by difference.
[d] **Calculated by Cordero et al. equation** [47].
[e] Value lower than 0.1.

chars tend to have higher C and lower H contents, Table 3. However, OL chars have high nitrogen content (up to 3.4 %), probably due to the presence of nitrogen compounds in the Organosolv process for generating this lignin, while KL-derived chars also present sulfur in their composition. The presence of heteroatoms is not desirable for biofuels but can be of interest for catalytic and energy applications [78].

On the other hand, the initial viability as C-sink and soil amend of these chars seems to be promising attending to the European Biochar Certification guidelines, given their high C content, especially those for chars obtained from high lignin content; the presence of K, Ca, N or Fe, (reaching values as high as 2.1 % m/m of K for AS, or 2.7 % m/m of Ca for HH, as can be seen in Table S10); and the low H/C ratios (an indication of the biochar stability), with values lower than 0.4 for all the bio-chars prepared at 600 and 800 °C, in compliance with the recommend value for EBC-FeedPlus certification. In this sense, it is also important to indicate that heavy metals (like Pb, Cd, Cu, Ni, Hg, Zn, Cr and As) were not detected by XRF (<0.01 % m/m) in any of the bio-char obtained.

Higher heating values (HHV) between 28.4 and 34.5 MJ/kg have been obtained for the different biochar (Table 3), achieving an overall net increase of 40–60 % for agricultural biomass (HH, OS and AS) and 17–45 % for the lignin-derived chars, when compared to the HHVs of the starting biomasses. This increase is strikingly higher if the HHV is expressed in volumetric terms using the bulk density of the chars, moving from 10.1 MJ/L for OS up to 28.8 MJ/L for the OS-derived bio-char pyrolyzed at 800 °C, or increasing 3.8 times for the HH after pyrolysis at 800 °C, highlighting the advantages of pyrolysis for improving the feasibility of using herbaceous plants as biofuels. HHVs are in line to those reported in the literature on chars derived from lignocellulosic biomass, which makes the bio-chars reported in this work suitable as solid biofuels [47,79].

Table 4 shows the textural parameters obtained from N_2 adsorption-desorption isotherms at −196 °C, and CO_2 adsorption isotherms at 0 °C (Figs. S2, S3, S4, S5 and S6). Biochars usually present narrow micropores with sizes below 0.7 nm [12], which cannot be properly analyzed using N_2 adsorption-desorption isotherms at −196 °C due to diffusional limitations at such low temperature. For this range of micropore sizes, the analysis of CO_2 adsorption at 0 °C is recommended [48,80]. Accordingly, all the biochars prepared in this work present very low values of A_{BET} and $V_{micro}^{N_2}$, with the latter value being always lower than the one derived from CO_2 isotherms, $V_{micro}^{CO_2}$, confirming that the average micropore size of these bio-chars is below 0.7 nm [50]. Therefore, all the bio-chars exhibit very narrow microporosity, enabling their potential as carbon molecular sieves.

The average pore size of the narrow micropore, $L_0^{CO_2}$, was calculated from the Stoeckli et al. equation (3) applied to the CO_2 adsorption isotherm [81], since some authors propose that the lower the value of $L_0^{CO_2}$, the higher the CO_2 adsorption capacity [82].Results from Table 4 show that the average pore size decreases with pyrolysis temperature, a trend that is also reflected in the A_{BET} values derived from the N_2 adsorption isotherm. This is connected to the porosity shrinkage produced by the structural rearrangement and ordering of the carbon matrix during the pyrolysis process, which leads to an increase in the narrower micropore at the expense of wider micropores, which prevents N_2 adsorption due to diffusional limitations at that low adsorption temperature (−196 °C), without achieving adsorption equilibrium within the analysis times of today's automatic adsorption equipment [80,83]. In this case, adsorption of CO_2 at considerable higher temperature (0 °C) is recommended, thus avoiding diffusional limitations, which leads to a larger value of (narrower) micropore volume ($V_{micro}^{CO_2}$) determined by the CO_2 adsorption isotherm at 0 °C. Among all the bio-chars generated, it could be expected that those obtained at 800 °C to be excellent candidates for the selective capture of carbon dioxide (CO_2). Results of 2D- NLDFT-derived CO_2 PSDs presented in Fig. 4 show additional differences in the pore network of these chars. OL derived bio-char presents a unimodal pore size distribution centered at ~4.5 Å, whereas for the rest of the porous carbon materials, a bimodal distribution can be observed, all sharing a peak centered at ~4.5 Å and another peak centered at larger micropore size, between 7.8 and 8.3 Å and increasing in amplitude, depending on the starting biomass (AS < KL < OS < HH) [84]. Therefore, wide micropores are more abundant in the biochar obtained from HH, followed by those from OS, KL and AS.

Thus, the contribution of wide micropore in the obtained biochars

Table 4
Textural parameters obtained from N_2 and CO_2 adsorption isotherms.

Char	Pyrolysis temperature	A_{BET}	$V_{micro}^{N_2}$	$V_{micro}^{CO_2}$	L_0 ^{CO_2}
	(°C)	(m^2/g)	(cm^3/g)	(cm^3/g)	(nm)
HH	**400**	12.0 ± 0.1	<0.01 ± 0.01	0.11 ± 0.01	0.55
	500	44.0 ± 1.0	0.02 ± 0.02	0.14 ± 0.01	0.54
	600	42.0 ± 1.0	0.02 ± 0.02	0.15 ± 0.01	0.52
	800	14.0 ± 0.2	<0.01 ± 0.01	0.19 ± 0.01	0.45
OS	**400**	1.0 ± 0.1	<0.01 ± 0.01	0.10 ± 0.01	0.65
	500	1.0 ± 0.1	<0.01 ± 0.01	0.14 ± 0.01	0.55
	600	22.0 ± 0.2	<0.01 ± 0.01	0.18 ± 0.01	0.55
	800	10.0 ± 0.2	<0.01 ± 0.01	0.20 ± 0.01	0.48
AS	**400**	<1.0 ± 0.1	<0.01 ± 0.01	0.09 ± 0.01	0.60
	500	1.0 ± 0.1	<0.01 ± 0.01	0.13 ± 0.01	0.52
	600	<1.0 ± 0.2	<0.01 ± 0.01	0.15 ± 0.01	0.46
	800	1.0 ± 0.1	<0.01 ± 0.01	0.17 ± 0.01	0.44
OL	**400**	<1.0 ± 0.1	<0.01 ± 0.01	0.08 ± 0.01	0.68
	500	<1.0 ± 0.1	<0.01 ± 0.01	0.09 ± 0.01	0.76
	600	2.0 ± 0.2	<0.01 ± 0.01	0.17 ± 0.01	0.59
	800	3.0 ± 0.2	<0.01 ± 0.01	0.21 ± 0.01	0.56
KL	**400**	3.0 ± 0.1	<0.01 ± 0.04	0.06 ± 0.01	–
	500	2.0 ± 0.1	<0.01 ± 0.03	0.11 ± 0.01	0.55
	600	1.0 ± 0.1	<0.01 ± 0.03	0.20 ± 0.01	0.53
	800	1.0 ± 0.1	<0.01 ± 0.02	0.17 ± 0.01	0.44

seems to be related to the amount of holocellulose in the starting material. The presence of a secondary wide micropore network can help in avoiding mass transfer limitations, making them more attractive for CO_2 capture in adsorption processes.

3.5.1. Gas separation studies

Dynamic adsorption-desorption studies simulating three different streams related to pyrolysis gases, hydrogen production and biogas upgrading were carried out on the bio-chars produced at 800 °C (HH-800, OS-800, AS-800, OL-800 and KL-800). As previously mentioned, the narrow microporosity of these samples matches the size requirements for selective CO_2 adsorption, though their unique PSDs can have different impacts in the adsorption process.

Fig. 5 shows the breakthrough curves at 25 °C for the different bio-chars prepared at a pyrolysis temperature of 800 °C, obtained using a gas mixture composed of 42 % CO_2, 32 % CO, 16 % H_2 and 10 % CH_4, which reflect the concentrations relative to those obtained in the pyrolysis gas stream, as described in section 3.4. The most relevant CO_2 adsorption parameters are also included in Table 5, for the sake of comparison.

The breakthrough curves demonstrate favorable behavior in CO_2 adsorption and separation, exhibiting superior BST for CO_2 adsorption, compared to the rest of the gases in the mixture, except for the OL-derived char, which presented similar values to those of the other gases and has not been considered for this study. A roll-up effect is observed for the CO, H_2 and CH_4 profiles, related to their faster adsorption rates when compared to CO_2, owing to their lower molecular kinetic diameters (0.38, 0.29 and 0.38 nm, respectively) [85]. After the adsorption of these gases, CO_2 reaches the adsorption sites at the narrow porosity and the former species are replaced due to the favored CO_2 adsorption, causing a shift and the release of these gases.

The CO_2 adsorption capacity of HH-800 and OS-800 is similar, showing values of 0.93 and 1.03 mmol/g, respectively, and considerable higher than that for AS-800 and KL-800, of 0.70 mmol/g. Moreover, the relevance of the adsorption kinetics, which is favored on bio-chars with larger amount of wide micropores, is clearly reflected in the column efficiency, where HH-800, showing an almost ideal step breakthrough profile, presents the highest efficiency, followed by OS-800, KL-800 and AS-800, (with values of 85.6 %, 66.7 %, 32.0 % and 25.7 %, respectively, Table 5), values that are clearly related to the amount of wide micropores (pore sized between 0.78 and 0.83 nm, Fig. 5) of the studied chars. An analysis of the kinetic selectivity of CO_2 in binary streams (CO_2/CH_4, CO_2/H_2 and CO_2/CO) and in quaternary stream (CO_2/CH_4, H_2, CO) has been performed, as detailed in Table 5. Values ranging between 10 and 53 have been recorded, depending on the gas and biochar used in the adsorption process. In particular the HH-derived biochar presents the highest selectivity for the CO_2/CH_4 separation, achieving significantly higher selectivity compared to the values reported in the literature, which usually range around 5 for activated carbon [52,86]. These results confirm the high potential of HH-800 for upgrading pyrolysis gases.

The purification of the pyrolysis gas stream through this process would result in a significant increase in the heating value (LHV), as shown in Fig. S8, enabling its application as fuel for internal combustion

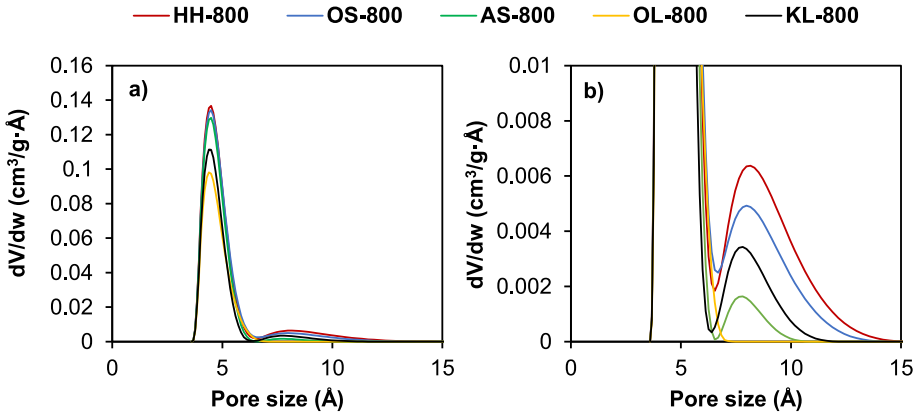

Fig. 4. Pore size distribution from CO_2 adsorption isotherm at 0 °C of the solid residue of the pyrolysis of HH, OS, AS, OL and KL at 800 °C.

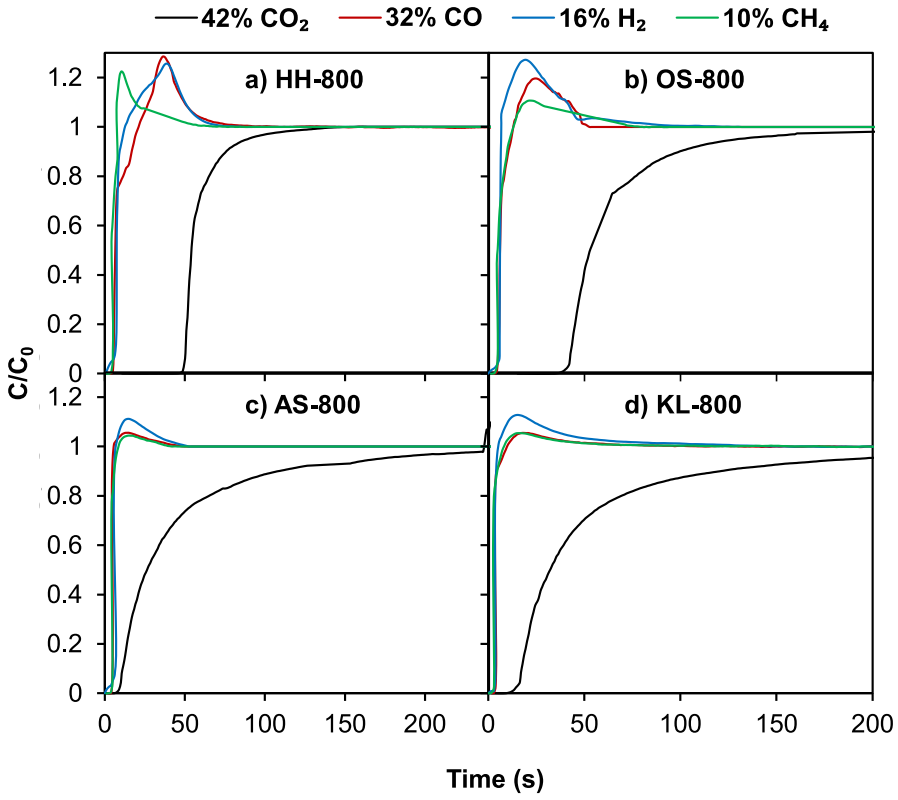

Fig. 5. Breakthrough curves at 25 °C, atmospheric pressure and a gas flow rate of 50 cm^3 STP/min of simulated pyrolysis gases mixture (CO_2, CO, H_2, CH_4) on chars HH (a), OS (b), AS (c) and KL (d) pyrolyzed at 800 °C.

Table 5
Parameter values from experimental adsorption breakthrough curves and selectivity ratio for HH, OS, AS and KL pyrolyzed at 800 °C.

	HH-800	OS-800	AS-800	KL-800
q_{CO_2} (mmol/g)	0.93	1.03	0.70	0.70
BST_{CO_2} (s)	51	44	12	14
q_{H_2} (mmol/g)	0.01	0.01	0.02	0.02
q_{CO} (mmol/g)	0.05	0.03	0.04	0.02
q_{CH_4} (mmol/g)	0.01	0.01	0.02	0.01
η (%)	85.6	66.7	25.7	32.0
S_{CO_2/CH_4}	52	43	10	14
S_{CO_2/H_2}	14	34	12	27
$S_{CO_2/CO}$	53	19	12	11
$S_{CO_2/(CH_4, H_2, CO)}$	21	29	12	17

engines. For the specific case of hemp residue-derived char, the one presenting the highest adsorption bed efficiency, an increase in the LHVs of the pyrolysis gases from 11 to 17 MJ/Nm^3 is observed. The others biochar derived from biomass residues used showed an increase of ca. 31, 41 and 12 % for OS, AS and KL, respectively.

Based on these results, biochar HH-800, which has a higher CO_2 adsorption capacity and the most significant column efficiency, was further tested in the separation of CO_2 from CH_4 in a simulated biogas stream and in the separation of CO_2 from H_2 from a simulated steam reforming stream (Fig. 6).

On the one hand, and based on literature data, for the biogas stream separation gas inlet compositions of 50–70 % CH_4 and 50-30 % CO_2 have been evaluated [87–89]. Focusing on the 50 % CH_4 and 50 % CO_2 gas composition, Fig. 6a presents the breakthrough separation profiles, which show quite low breakthrough time for the methane, compared to that for CO_2, confirming the high selectivity for CO_2 capture of this bio-char. The BSTs of methane are further reduced as CH_4 concentration increases, Fig. 6b and c. In all cases, the huge difference between breakthrough times ensures an adequate separation of CO_2 from CH_4. In addition, it is observed that as the CO_2 concentration increases, not only is a higher adsorption capacity achieved (1.61, 1.12 and 1.05 mmol/g for a CO_2 concentration of 50, 40 and 30 %, respectively), but also the kinetic rate of the process is improved, as depicted by the shape of the breakthrough profile. Consequently, a strong increase in column efficiency from 83.8 to 98.5 % is attained when the CO_2 concentration varies from 30 to 50 %. The CO_2/CH_4 selectivity coefficient for the equimolecular mixture is 5, being higher than those reported in the literature [52,86,90]. Reducing the CO_2 concentration down to 40 and 30 % renders CO_2/CH_4 values of 10 and 12, validating the performance of HH-800 as a potential selective CO_2 adsorbent for upgrading biogas streams.

On the other hand, the separation of CO_2 and H_2 in a simulated steam reforming stream has also been studied on HH-800 char. For this study, different steam reforming stream compositions have been analyzed (gas stream is composed of CO_2 and H_2, where CO_2/H_2 ratios of 25/75, 50/50 and 75/25 have been used). For all the mixtures tested in the gas stream, the breakthrough time for H_2 is shorter than that for CO_2, Fig. 6d and e and f, confirming that it is possible to selectively capture CO_2 from a CO_2/H_2 stream, producing a stream of pure H_2 at the exit of the adsorption column. Although the breakthrough times for both gases get closer as H_2 concentration increases, Fig. 6e and f, the roll-up effect of H_2 greatly decreases the amount of this gas adsorbed on the porosity of the char when the CO_2 breakthrough time is achieved. Consequently, the selectivity of the CO_2 capture shows again high values (increasing from 6 to 21 as CO_2 concentration decreases). Additionally, the presence of hydrogen in the gas stream seems to have a reduced impact, meaning that the column efficiency shows only marginal changes in the operation conditions tested in this study.

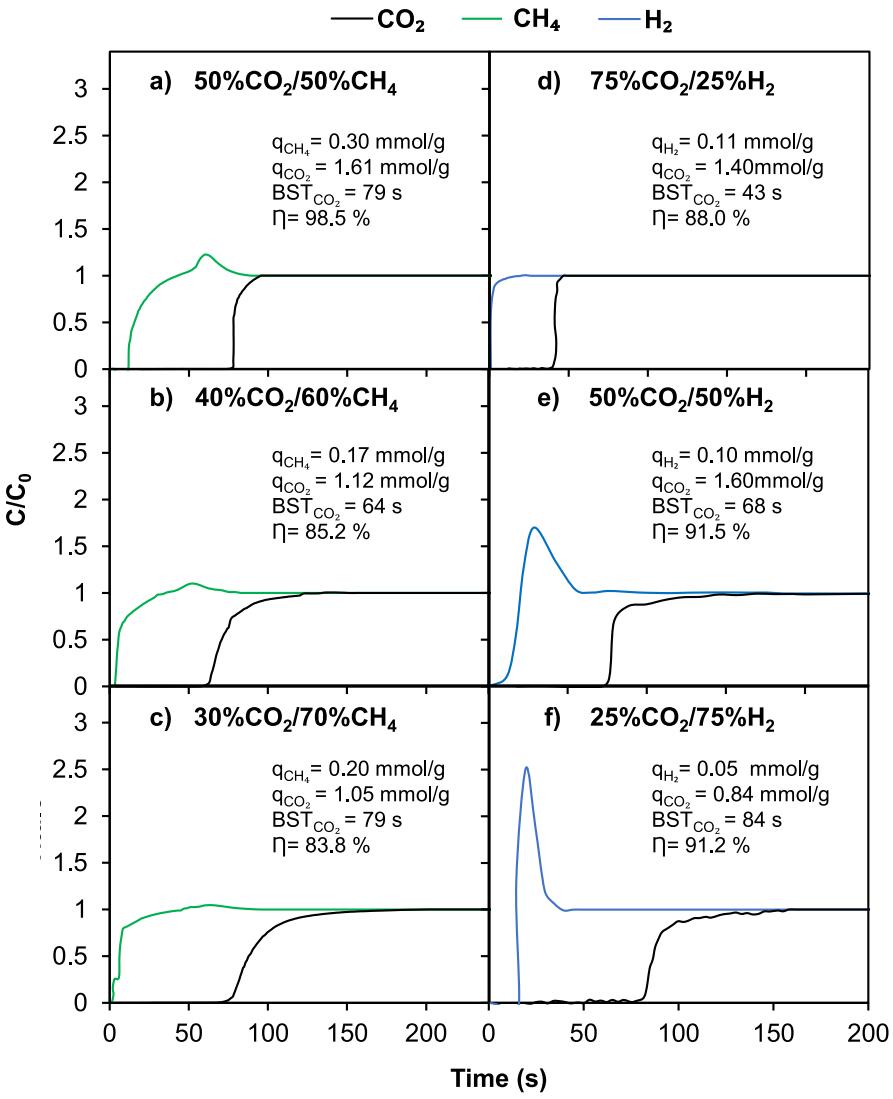

Fig. 6. Parameters for the experimental breakthrough adsorption curves of simulated biogas (CO_2, CH_4) and steam reforming (CO_2, H_2) streams on HH-800, using a) 50 % CO_2, b) 40 % CO_2, c) 30 % CO_2 and CH_4 as balance, and d) 75 % CO_2, e) 50 % CO_2 and f) 25 % CO_2 and H_2 as balance, respectively.

Lastly, the regeneration of the adsorbent is necessary for enabling steady operation of a CO_2 capture process based in adsorption. A complete desorption of the CO_2 and the rest of the gases was attained in all the gas separation studies carried out in this work (see Fig. S7 as an example of desorption process for HH-800 biochar saturated with a gas pyrolysis stream, by using a flow rate of 50 cm^3 STP/min of Ar). These results confirm that bio-chars reported in this work could be good candidates as adsorbent for CO_2 removal in a pressure swing adsorption process.

3.6. Determination of the minimum selling price of pyrolysis products and costs of biomass residues for a cost-benefit analysis

Technoeconomic analysis is a powerful tool to establish the financial viability of chemical processes based on different technologies or product options. Deep technoeconomic analyses demand establishing a detailed process simulation and gathering a collection of experimental and industrial data which are beyond the scope of this work [91]. As a prior baseline for such analyses, the potential economic benefits of the different lignocellulosic biomass have been roughly calculated from proximate biomass costs and the minimum selling prices of the main products. The minimum selling prices (MSPs) have been combined with the conversion yields for each product in order to obtain a total selling price of the pyrolysis process and matched against the cost of the corresponding lignocellulosic biomass. Details about how the MSPs have been fixed and the sources for estimating the costs and the MSPs of the products have been included in the supplementary file. The results have been summarized in Table 6. The difference between total selling prices and biomass costs indicates that the benefits are potentially higher in the case of Kraft lignin, achieving a value of 474 €/tonne. Note that this analysis does not include the cost of bio-oil fractionation, which is expected to rule out any potential benefit of their commercialization. As the pyrolysis of kraft lignin is highly reliant on the oil selling prices of the compounds in the bio-oil, it is envisaged that AS could achieve higher benefits owing to a combination of high selling prices of biochar and thermal energy from the gas stream.

4. Conclusions

The slow pyrolysis of five agro-lignocellulosic residues (HH, OS, AS, OL, and KL) was studied between 400 and 800 °C to assess their potential for high-value products.

Table 6
Economic balance estimate of the pyrolysis of the different biomass values at 800 °C.

Biomass	Biomass cost (€/tonne)[1]	Selling Prices Biochar (€/tonne)	Selling Prices Bio-oil (€/tonne)	Selling Prices Biogas (€/tonne)	Benefits (€/tonne)
Hemp Hurd (HH)	192 [a]	128	126	158	220
Olive Stone (OS)	294 [b]	196	140	167	209
Almond Shell (AS)	96 [c]	189	102	167	362
Organosolv Lignin (OL)	400 [d]	355	42	197	194
Kraft Lignin (KL)	380 [d]	358	295	201	474

[1a] source [92]
[1b] source [93]
[1c] source [94]
[1d] source [95]

KL proved the most promising for renewable aromatics and bio-oil due to low water and acid production and high aromatic yields. In contrast, HH's liquid fraction, rich in hydrogen and water, showed potential for hydrogen production via steam reforming. AS and OL were less suitable for bio-oil production. Liquid yield increased with temperature, peaking in HH due to its high holocellulose content.

The gas fraction, mainly CO and CO_2, showed more CH_4 and H_2 at higher temperatures and with increased lignin content. LHV of gas shows a maximum value at 500 °C for the lignin feedstocks.

The solid products exhibited high HHVs and bimodal microporosity containing narrow and wide micropores. The higher the holocellulose content of the biomass feedstock, the higher the average size and the greater the abundance of wide micropores in the resulting bio-char. These wide micropores improved the adsorption kinetics of CO_2 on the bio-chars and, thus, the selective removal in dynamic fixed-bed adsorption columns. HH and OS bio-chars demonstrate superior performance on CO_2 removal, aiding its separation from pyrolysis gas, biogas, and reforming streams.

Bio-chars, particularly from high-lignin biomass, had high C content, essential nutrients (K, N, Ca), and low H/C ratios, making them promising not only for CO_2 adsorption but also as C-sinks or soil amendments under European Bio-char Certification guidelines. Their use in the latter applications could enhance pyrolysis sustainability within a circular economy by improving soil quality and sequestering carbon.

CRediT authorship contribution statement

María del Carmen Recio-Ruiz: Writing – original draft, Visualization, Methodology, Investigation, Formal analysis, Conceptualization. **Ramiro Ruiz-Rosas:** Writing – original draft, Supervision, Methodology, Formal analysis. **Francisco José García-Mateos:** Visualization, Investigation, Formal analysis. **María José Valero-Romero:** Writing – original draft, Methodology, Formal analysis. **Juana María Rosas:** Supervision, Project administration, Methodology, Funding acquisition. **José Rodríguez-Mirasol:** Writing – review & editing, Supervision, Project administration, Methodology, Funding acquisition. **Tomás Cordero:** Writing – review & editing, Supervision, Project administration, Methodology, Investigation, Conceptualization.

Acknowledges

This work was supported by MCIN [TED2021-131324B-C21; PID2022-140844OB-I00] and European Union "NextGenerationEU"/PRTR (MCIN/AEI/10.13039/501100011033); M.C.R.R. thanks MINECO for financial support (PRE2019-089340), and "II Plan Propio de Investigación, Transferencia y Divulgación Científica" of Universidad de Málaga.

Appendix A. Supplementary data

Supplementary data to this article can be found online at https://doi.org/10.1016/j.biombioe.2025.107676.

Data availability

No data was used for the research described in the article.

References

[1] Y. Li, R. Gupta, Q. Zhang, S. You, Review of biochar production via crop residue pyrolysis: development and perspectives, Bioresour. Technol. 369 (2023) 128423, https://doi.org/10.1016/j.biortech.2022.128423.
[2] S.-K. Cho, B. Igliński, G. Kumar, Biomass based biochar production approaches and its applications in wastewater treatment, machine learning and microbial sensors, Bioresour. Technol. 391 (2024) 129904, https://doi.org/10.1016/j.biortech.2023.129904.
[3] W. Lan, X. Zhao, Y. Wang, X. Jin, J. Ji, Z. Cheng, G. Yang, H. Li, G. Chen, Research progress of biochar modification technology and its application in environmental remediation, Biomass Bioenergy 184 (2024) 107178, https://doi.org/10.1016/J.BIOMBIOE.2024.107178.
[4] M.J. Antal, M. Grønli, The art, science, and technology of charcoal production, Ind. Eng. Chem. Res. 42 (2003) 1619–1640, https://doi.org/10.1021/ie0207919.
[5] S. Adhikari, E. Moon, J. Paz-Ferreiro, W. Timms, Comparative analysis of biochar carbon stability methods and implications for carbon credits, Sci. Total Environ. 914 (2024) 169607, https://doi.org/10.1016/j.scitotenv.2023.169607.
[6] K. Qian, A. Kumar, H. Zhang, D. Bellmer, R. Huhnke, Recent advances in utilization of biochar, Renew. Sustain. Energy Rev. 42 (2015) 1055–1064, https://doi.org/10.1016/j.rser.2014.10.074.
[7] F.M. Muema, Y. Richardson, A. Keita, M. Sawadogo, An interdisciplinary overview on biochar production engineering and its agronomic applications, Biomass Bioenergy 190 (2024) 107416, https://doi.org/10.1016/J.BIOMBIOE.2024.107416.
[8] European Commission, COMMITTEE and the committee of the regions towards an ambitious industrial carbon management for the EU. https://eur-lex.europa.eu/legal-content/EN/TXT/?uri=COM%3A2024%3A62%3AFIN, 2024. (Accessed 23 May 2024).
[9] Carbon Standards International AG, The European biochar certificate (EBC), n.d. https://www.european-biochar.org/en, 2024. (Accessed 23 May 2024).
[10] M. Garcia-Perez, A. Chaala, H. Pakdel, D. Kretschmer, C. Roy, Characterization of bio-oils in chemical families, Biomass Bioenergy 31 (2007) 222–242, https://doi.org/10.1016/J.BIOMBIOE.2006.02.006.
[11] A.V. Bridgwater, Review of fast pyrolysis of biomass and product upgrading, Biomass Bioenergy 38 (2012) 68–94, https://doi.org/10.1016/J.BIOMBIOE.2011.01.048.
[12] E.M. Calvo-Muñoz, F.J. García-Mateos, J.M. Rosas, J. Rodríguez-Mirasol, T. Cordero, Biomass waste carbon materials as adsorbents for CO2 capture under post-combustion conditions, Front. Mater. 3 (2016), https://doi.org/10.3389/fmats.2016.00023.
[13] E.I. Koytsoumpa, D. Magiri – Skouloudi, S. Karellas, E. Kakaras, Bioenergy with carbon capture and utilization: a review on the potential deployment towards a European circular bioeconomy, Renew. Sustain. Energy Rev. 152 (2021) 111641, https://doi.org/10.1016/J.RSER.2021.111641.
[14] P. Basu, Biomass gasification and pyrolysis; chapter 3 pyrolysis and torrefaction, in: Biomass Gasification Design Handbook, Elsevier, 2010, pp. 65–96, https://doi.org/10.1016/b978-0-12-374988-8.00003-9.
[15] N. Agnihotri, M.K. Mondal, Process parameter variation of Melia azedarach sawdust pyrolysis for fuel properties, physicochemical characterization, and in-depth speciation analysis, Biomass Convers Biorefin. 1 (2023) 1–15, https://doi.org/10.1007/S13399-023-04305-7.
[16] U. Epple, H.A. Schneider, Glass transition behaviour of acrylic donor or acceptor copolymers - homopolymers and their polymer blends with EDA complexation, Thermochim. Acta 160 (1990) 103–112, https://doi.org/10.1016/0040-6031(90)80250-3.
[17] R. Bilbao, A. Millera, J. Arauzo, Product distribution in the flash pyrolysis of lignocellulosic materials in a fluidized bed, Fuel 67 (1988) 1586–1588, https://doi.org/10.1016/0016-2361(88)90082-8.
[18] R. Bilbao, A. Millera, J. Arauzo, Kinetics of weight loss by thermal decomposition of xylan and lignin. Influence of experimental conditions, Thermochim. Acta 143 (1989) 137–148, https://doi.org/10.1016/0040-6031(89)85051-8.
[19] R. Bilbao, A. Millera, J. Arauzo, Thermal decomposition of lignocellulosic materials: influence of the chemical composition, Thermochim. Acta 143 (1989) 149–159, https://doi.org/10.1016/0040-6031(89)85052-X.
[20] R. Bilbao, M.L. Salvador, J. Arauzo, Influence of the heating rate on the temperature profiles and on the conversion rate of powdery cellulose and pine sawdust, J. Anal. Appl. Pyrolysis 30 (1994) 145–159, https://doi.org/10.1016/0165-2370(94)00809-4.

[21] R. Bilbao, J. Arauzo, M.L. Salvador, Kinetics and modeling of gas formation in the thermal decomposition of powdery cellulose and pine sawdust, Ind. Eng. Chem. Res. 34 (1995) 786–793, https://doi.org/10.1021/ie00042a010.
[22] R. Bilbao, A. Millera, M.B. Murillo, Temperature profiles and weight loss in the thermal decomposition of large spherical wood particles, Ind. Eng. Chem. Res. 32 (1993) 1811–1817, https://doi.org/10.1021/ie00021a003.
[23] R. Bilbao, M.L. Salvador, P. Garcia, J. Arauzo, Solid weight loss in the thermal decomposition of cellulose and pine sawdust, J. Anal. Appl. Pyrolysis 24 (1993) 257–271, https://doi.org/10.1016/0165-2370(93)85005-J.
[24] R. Bilbao, M.B. Murillo, A. Millera, Angular and radial temperature profiles in the thermal decomposition of wood, Thermochim. Acta 200 (1992) 401–411, https://doi.org/10.1016/0040-6031(92)85133-G.
[25] R. Bilbao, M.B. Murillo, A. Millera, J.F. Mastral, Thermal decomposition of lignocellulosic materials: comparison of the results obtained in different experimental systems, Thermochim. Acta 190 (1991) 163–173, https://doi.org/10.1016/0040-6031(91)85242-A.
[26] T.Y.A. Fahmy, Y. Fahmy, F. Mobarak, M. El-Sakhawy, R.E. Abou-Zeid, Biomass pyrolysis: past, present, and future, Environ. Dev. Sustain. 22 (2020) 17–32, https://doi.org/10.1007/s10668-018-0200-5.
[27] M.J. Antal, W.S.L. Mok, G. Varhegyi, T. Szekely, Review of methods for improving the yield of charcoal from biomass, Energy Fuels 4 (1990) 221–225, https://doi.org/10.1021/ef00021a001.
[28] S. Wang, G. Dai, H. Yang, Z. Luo, Lignocellulosic biomass pyrolysis mechanism: a state-of-the-art review, Prog. Energy Combust. Sci. 62 (2017) 33–86, https://doi.org/10.1016/J.PECS.2017.05.004.
[29] A. Tomczyk, Z. Sokołowska, P. Boguta, Biochar physicochemical properties: pyrolysis temperature and feedstock kind effects, Rev. Environ. Sci. Biotechnol. 19 (2020) 191–215, https://doi.org/10.1007/s11157-020-09523-3.
[30] M. Amutio, G. Lopez, J. Alvarez, R. Moreira, G. Duarte, J. Nunes, M. Olazar, J. Bilbao, Flash pyrolysis of forestry residues from the Portuguese Central Inland Region within the framework of the BioREFINA-Ter project, Bioresour. Technol. 129 (2013) 512–518, https://doi.org/10.1016/J.BIORTECH.2012.11.114.
[31] I. Garcia, G. Lopez, L. Santamaria, E. Fernandez, J. Bilbao, M. Olazar, M. Artetxe, M. Amutio, Biomass source influence on hydrogen production through pyrolysis and in line oxidative steam reforming, ChemSusChem 17 (2024), https://doi.org/10.1002/CSSC.202400325.
[32] H. Hernando, G. Gómez-Pozuelo, J.A. Botas, D.P. Serrano, Evaluating fractional pyrolysis for bio-oil speciation into holocellulose and lignin derived compounds, J. Anal. Appl. Pyrolysis 154 (2021) 105019, https://doi.org/10.1016/J.JAAP.2021.105019.
[33] S.D. Stefanidis, K.G. Kalogiannis, E.F. Iliopoulou, C.M. Michailof, P.A. Pilavachi, A. A. Lappas, A study of lignocellulosic biomass pyrolysis via the pyrolysis of cellulose, hemicellulose and lignin, J. Anal. Appl. Pyrolysis 105 (2014) 143–150, https://doi.org/10.1016/j.jaap.2013.10.013.
[34] H. Yang, R. Yan, H. Chen, D.H. Lee, C. Zheng, Characteristics of hemicellulose, cellulose and lignin pyrolysis, Fuel 86 (2007) 1781–1788, https://doi.org/10.1016/j.fuel.2006.12.013.
[35] K.N. Yogalakshmi, T. Poornima Devi, P. Sivashanmugam, S. Kavitha, R. Yukesh Kannah, V. Sunita, S. AdishKumar, K. Gopalakrishnan, J. Rajesh Banu, Lignocellulosic biomass-based pyrolysis: a comprehensive review, Chemosphere 286 (2022) 131824, https://doi.org/10.1016/J.CHEMOSPHERE.2021.131824.
[36] A.T.M.F. Ahmed, M.Z. Islam, M.S. Mahmud, M.E. Sarker, M.R. Islam, Hemp as a potential raw material toward a sustainable world: a review, Heliyon 8 (2022) e08753, https://doi.org/10.1016/j.heliyon.2022.e08753.
[37] F.P. Gomez, J. Hu, M.A. Clarke, Cannabis as a feedstock for the production of chemicals, fuels, and materials: a review of relevant studies to date, Energy Fuel. 35 (2021) 5538–5557, https://doi.org/10.1021/acs.energyfuels.0c04121.
[38] S. Liu, L. Ge, S. Gao, L. Zhuang, Z. Zhu, H. Wang, Activated carbon derived from bio-waste hemp hurd and retted hemp hurd for CO_2 adsorption, Compos. Commun. 5 (2017) 27–30, https://doi.org/10.1016/j.coco.2017.06.002.
[39] F. Mirizzi, V. Troyano, Hemp cultivation & production in Europe in 2018. https://eiha.org/wp-content/uploads/2020/10/2018-Hemp-agri-report.pdf, 2018. (Accessed 25 May 2024).
[40] J.B.D. Osei, A. Amiri, J. Wang, M.T. Tavares, W. Kiatkittipong, V. Najdanovic-Visak, Recovery of oils and antioxidants from olive stones, Biomass Bioenergy 166 (2022) 106623, https://doi.org/10.1016/j.biombioe.2022.106623.
[41] INC - International Nut&DriedFruit, Nuts & Dried Fruits Statistical Yearbook 2022/2023, 2023.
[42] S. Sethupathy, G. Murillo Morales, L. Gao, H. Wang, B. Yang, J. Jiang, J. Sun, D. Zhu, Lignin valorization: status, challenges and opportunities, Bioresour. Technol. 347 (2022) 126696, https://doi.org/10.1016/j.biortech.2022.126696.
[43] L. Dessbesell, M. Paleologou, M. Leitch, R. Pulkki, C.Charles Xu, Global lignin supply overview and kraft lignin potential as an alternative for petroleum-based polymers, Renew. Sustain. Energy Rev. 123 (2020) 109768, https://doi.org/10.1016/j.rser.2020.109768.
[44] R.M. Rowell, Handbook of Wood Chemistry and Wood Composites, second ed., CRC Press, Boca Raton, 2013.
[45] E. Christensen, J. Ferrell, M. V Olarte, A.B. Padmaperuma, Quantification of semi-volatile oxygenated components of pyrolysis bio-oil by gas chromatography/mass Spectrometry (GC/MS), Lab. Anal. Proc. (LAP) (2016). www.nrel.gov/publications.
[46] M. Gräbner, Industrial Coal Gasification Technologies Covering Baseline and High-Ash Coal, 2015.
[47] T. Cordero, F. Marquez, J. Rodriguez-Mirasol, J. Rodriguez, Predicting heating values of lignocellulosics and carbonaceous materials from proximate analysis, Fuel 80 (2001) 1567–1571, https://doi.org/10.1016/S0016-2361(01)00034-5.
[48] M. Thommes, K. Kaneko, A.V. Neimark, J.P. Olivier, F. Rodriguez-Reinoso, J. Rouquerol, K.S.W. Sing, Physisorption of gases, with special reference to the evaluation of surface area and pore size distribution (IUPAC Technical Report), Pure Appl. Chem. 87 (2015) 1051–1069, https://doi.org/10.1515/pac-2014-1117.
[49] J. Jagiello, C. Ania, J.B. Parra, C. Cook, Dual gas analysis of microporous carbons using 2D-NLDFT heterogeneous surface model and combined adsorption data of N_2 and CO_2, Carbon 91 (2015) 330–337, https://doi.org/10.1016/J.CARBON.2015.05.004.
[50] D. Cazorla-Amorós, J. Alcañiz-Monge, M.A. de la Casa-Lillo, A. Linares-Solano, CO_2 as an adsorptive to characterize carbon molecular sieves and activated carbons, Langmuir 14 (1998) 4589–4596, https://doi.org/10.1021/la980198p.
[51] H.F. Stoeckli, P. Rebstein, L. Ballerini, On the assessment of microporosity in active carbons, a comparison of theoretical and experimental data, Carbon 28 (1990) 907–909, https://doi.org/10.1016/0008-6223(90)90339-Z.
[52] I. Durán, N. Álvarez-Gutiérrez, F. Rubiera, C. Pevida, Biogas purification by means of adsorption on pine sawdust-based activated carbon: impact of water vapor, J. Chem. Eng. 353 (2018) 197–207, https://doi.org/10.1016/j.cej.2018.07.100.
[53] M.I. Jahirul, M.G. Rasul, A.A. Chowdhury, N. Ashwath, Biofuels production through biomass pyrolysis —a technological review, Energies 5 (2012) 4952–5001, https://doi.org/10.3390/en5124952.
[54] M. Mierzwa-Hersztek, K. Gondek, M. Jewiarz, K. Dziedzic, Assessment of energy parameters of biomass and biochars, leachability of heavy metals and phytotoxicity of their ashes, J. Mater. Cycles Waste Manag. 21 (2019) 786–800, https://doi.org/10.1007/s10163-019-00832-6.
[55] L. Zhou, Y. Jia, T.-H. Nguyen, A.A. Adesina, Z. Liu, Hydropyrolysis characteristics and kinetics of potassium-impregnated pine wood, Fuel Process. Technol. 116 (2013) 149–157, https://doi.org/10.1016/j.fuproc.2013.05.005.
[56] K. Haddad, M. Jeguirim, S. Jellali, C. Guizani, L. Delmotte, S. Bennici, L. Limousy, Combined NMR structural characterization and thermogravimetric analyses for the assessment of the AAEM effect during lignocellulosic biomass pyrolysis, Energy 134 (2017) 10–23, https://doi.org/10.1016/j.energy.2017.06.022.
[57] A. Oasmaa, Y. Solantausta, V. Arpiainen, E. Kuoppala, K. Sipilä, Fast pyrolysis bio-oils from wood and agricultural residues, Energy Fuel. 24 (2010) 1380–1388, https://doi.org/10.1021/ef901107f.
[58] T. Cordero, J.M. Rodríguez-Maroto, J. Rodríguez-Mirasol, J.J. Rodríguez, On the kinetics of thermal decomposition of wood and wood components, Thermochim. Acta 164 (1990) 135–144, https://doi.org/10.1016/0040-6031(90)80430-7.
[59] N. Agnihotri, G.K. Gupta, M.K. Mondal, Thermo-kinetic analysis, thermodynamic parameters and comprehensive pyrolysis index of Melia azedarach sawdust as a genesis of bioenergy, Biomass Convers Biorefin. 14 (2024) 1863–1880, https://doi.org/10.1007/S13399-022-02524-Y.
[60] T. Faravelli, A. Frassoldati, G. Migliavacca, E. Ranzi, Detailed kinetic modeling of the thermal degradation of lignins, Biomass Bioenergy 34 (2010) 290–301, https://doi.org/10.1016/J.BIOMBIOE.2009.10.018.
[61] S. Hameed, A. Sharma, V. Pareek, H. Wu, Y. Yu, A review on biomass pyrolysis models: kinetic, network and mechanistic models, Biomass Bioenergy 123 (2019) 104–122, https://doi.org/10.1016/J.BIOMBIOE.2019.02.008.
[62] F. Quesada-Plata, R. Ruiz-Rosas, E. Morallón, D. Cazorla-Amorós, Activated carbons prepared through H_3PO_4 -assisted hydrothermal carbonisation from biomass wastes: porous texture and electrochemical performance, Chempluschem 81 (2016) 1349–1359, https://doi.org/10.1002/cplu.201600412.
[63] J.J.M. Orfão, F.J.A. Antunes, J.L. Figueiredo, Pyrolysis kinetics of lignocellulosic materials—three independent reactions model, Fuel 78 (1999) 349–358, https://doi.org/10.1016/S0016-2361(98)00156-2.
[64] F. Sánchez, G. San Miguel, Improved fuel properties of whole table olive stones via pyrolytic processing, Biomass Bioenergy 92 (2016) 1–11, https://doi.org/10.1016/J.BIOMBIOE.2016.06.001.
[65] X. Li, Y. Liu, J. Hao, W. Wang, Study of almond shell characteristics, Materials 11 (2018), https://doi.org/10.3390/ma11091782.
[66] D. Mohan, C.U. Pittman, P.H. Steele, Pyrolysis of wood/biomass for bio-oil: a critical review, Energy Fuel. 20 (2006) 848–889, https://doi.org/10.1021/ef0502397.
[67] M. García-Rollán, M. Toscano-de los Riscos, R. Ruiz-Rosas, J.M. Rosas, J. Rodríguez-Mirasol, T. Cordero, Oxidative electrochemical depolymerization of lignin using highly active self-standing electrocatalysts prepared by electrospinning of lignin, Biomass Bioenergy 193 (2025) 107560, https://doi.org/10.1016/j.biombioe.2024.107560.
[68] H. Kawamoto, Lignin pyrolysis reactions, J. Wood Sci. 63 (2017) 117–132, https://doi.org/10.1007/s10086-016-1606-z.
[69] N. Agnihotri, M.K. Mondal, Thermal analysis, kinetic behavior, reaction modeling, and comprehensive pyrolysis index of soybean stalk pyrolysis, Biomass Convers Biorefin. 14 (2024) 14977–14992, https://doi.org/10.1007/S13399-023-03807-8.
[70] T. Cordero-Lanzac, J. Rodríguez-Mirasol, T. Cordero, J. Bilbao, Advances and challenges in the valorization of bio-oil: hydrodeoxygenation using carbon-supported catalysts, Energy Fuel. 35 (2021) 17008–17031, https://doi.org/10.1021/acs.energyfuels.1c01700.
[71] C. Zhao, E. Jiang, A. Chen, Volatile production from pyrolysis of cellulose, hemicellulose and lignin, J. Energy Inst. 90 (2017) 902–913, https://doi.org/10.1016/j.joei.2016.08.004.
[72] C. Di Blasi, G. Signorelli, C. Di Russo, G. Rea, Product distribution from pyrolysis of wood and agricultural residues, Ind. Eng. Chem. Res. 38 (1999) 2216–2224, https://doi.org/10.1021/IE980711U.
[73] H. Marsh, F. Rodríguez-Reinoso, Activated Carbon, Activated Carbon, 2006, pp. 1–536, https://doi.org/10.1016/B978-0-08-044463-5.X5013-4.
[74] J.L. Toro-Trochez, D.A. De Haro Del Río, L. Sandoval-Rangel, D. Bustos-Martínez, F.J. García-Mateos, R. Ruiz-Rosas, J. Rodríguez-Mirasol, T. Cordero, E.S. Carrillo-

Pedraza, Catalytic fast pyrolysis of soybean hulls: focus on the products, J. Anal. Appl. Pyrolysis 163 (2022) 105492, https://doi.org/10.1016/j.jaap.2022.105492.
[75] M. Zhu, I.E. Wachs, Iron-based catalysts for the high-temperature water–gas shift (HT-WGS) reaction: a review, ACS Catal. 6 (2016) 722–732, https://doi.org/10.1021/acscatal.5b02594.
[76] M. Van de Velden, J. Baeyens, A. Brems, B. Janssens, R. Dewil, Fundamentals, kinetics and endothermicity of the biomass pyrolysis reaction, Renew. Energy 35 (2010) 232–242, https://doi.org/10.1016/j.renene.2009.04.019.
[77] D.E. Daugaard, R.C. Brown, Enthalpy for pyrolysis for several types of biomass, Energy Fuel. 17 (2003) 934–939, https://doi.org/10.1021/ef020260x.
[78] Z. Wan, Y. Sun, D.C.W. Tsang, E. Khan, A.C.K. Yip, Y.H. Ng, J. Rinklebe, Y.S. Ok, Customised fabrication of nitrogen-doped biochar for environmental and energy applications, Chem. Eng. J. 401 (2020) 126136, https://doi.org/10.1016/j.cej.2020.126136.
[79] L. Aguiar, F. Márquez-Montesinos, A. Gonzalo, J.L. Sánchez, J. Arauzo, Influence of temperature and particle size on the fixed bed pyrolysis of orange peel residues, J. Anal. Appl. Pyrolysis 83 (2008) 124–130, https://doi.org/10.1016/J.JAAP.2008.06.009.
[80] W. Suliman, J.B. Harsh, N.I. Abu-Lail, A.M. Fortuna, I. Dallmeyer, M. Garcia-Perez, Influence of feedstock source and pyrolysis temperature on biochar bulk and surface properties, Biomass Bioenergy 84 (2016) 37–48, https://doi.org/10.1016/J.BIOMBIOE.2015.11.010.
[81] H.F. Stoeckli, P. Rebstein, L. Ballerini, On the assessment of microporosity in active carbons, a comparison of theoretical and experimental data, Carbon 28 (1990) 907–909, https://doi.org/10.1016/0008-6223(90)90339-Z.
[82] N. Querejeta, M.G. Plaza, F. Rubiera, C. Pevida, Water vapor adsorption on biomass based carbons under post-combustion CO_2 capture conditions: effect of post-treatment, Materials 9 (2016), https://doi.org/10.3390/ma9050359.
[83] F.J. García-Mateos, J.M. Rosas, R. Ruiz-Rosas, J. Rodríguez-Mirasol, T. Cordero, Highly porous and conductive functional carbon fibers from electrospun phosphorus-containing lignin fibers, Carbon 200 (2022) 134–148, https://doi.org/10.1016/j.carbon.2022.08.050.
[84] D. Jimenez-Cordero, F. Heras, N. Alonso-Morales, M.A. Gilarranz, J.J. Rodriguez, Porous structure and morphology of granular chars from flash and conventional pyrolysis of grape seeds, Biomass Bioenergy 54 (2013) 123–132, https://doi.org/10.1016/J.BIOMBIOE.2013.03.020.
[85] D.M. D'Alessandro, B. Smit, J.R. Long, Carbon dioxide capture: prospects for new materials, Angew. Chem. Int. Ed. 49 (2010) 6058–6082, https://doi.org/10.1002/anie.201000431.
[86] N. Querejeta, V. Gil, F. Rubiera, C. Pevida, Prospects of low-temperature solid sorbents in industrial CO_2 capture: a focus on biomass residues as precursor material. Greenh Gases, 2023, https://doi.org/10.1002/ghg.2210.
[87] K. Gallucci, L. Taglieri, A.A. Papa, F. Di Lauro, Z. Ahmad, A. Gallifuoco, Non-energy valorization of residual biomasses via HTC: CO_2 capture onto activated hydrochars, Appl. Sci. 10 (2020), https://doi.org/10.3390/app10051879.
[88] S. Jain, S. Jain, I.T. Wolf, J. Lee, Y.W. Tong, A comprehensive review on operating parameters and different pretreatment methodologies for anaerobic digestion of municipal solid waste, Renew. Sustain. Energy Rev. 52 (2015) 142–154, https://doi.org/10.1016/j.rser.2015.07.091.
[89] M. Karimi, A. Ferreira, A.E. Rodrigues, F. Nouar, C. Serre, J.A.C. Silva, MIL-160(Al) as a candidate for biogas upgrading and CO_2 capture by adsorption processes, Ind. Eng. Chem. Res. 62 (2023) 5216–5229, https://doi.org/10.1021/acs.iecr.2c04150.
[90] P.C. Vilella, J.A. Lira, D.C.S. Azevedo, M. Bastos-Neto, R. Stefanutti, Preparation of biomass-based activated carbons and their evaluation for biogas upgrading purposes, Ind. Crops Prod. 109 (2017) 134–140, https://doi.org/10.1016/j.indcrop.2017.08.017.
[91] M.R. Patel, N.L. Panwar, Evaluating the agronomic and economic viability of biochar in sustainable crop production, Biomass Bioenergy 188 (2024) 107328, https://doi.org/10.1016/J.BIOMBIOE.2024.107328.
[92] S.W. Selkirk, R.D. Spencer, Economics of fibre production from industrial hemp and blue gum plantations, Aust. For. 62 (1999) 193–201, https://doi.org/10.1080/00049158.1999.10674782.
[93] Asociación Española de biomasa, Índice de precios de HUESO de ACEITUNA para uso doméstico en España, n.d, www.avebiom.org. (Accessed 31 January 2025).
[94] R. Meadows, Almond waste is a growing challenge, ACS Cent. Sci. 9 (2023) 2171–2174, https://doi.org/10.1021/ACSCENTSCI.3C01458/ASSET/IMAGES/LARGE/OC3C01458_0006.JPEG.
[95] H. Ľudmila, J. Michal, Š. Andrea, H. Aleš, LIGNIN, potential products and their market value, n.d. chrome-extension://efaidnbmnnnibpcajpcglclefindmkaj/https://www.woodresearch.sk/wr/201506/13.pdf. (Accessed 31 January 2025).